

Practical Control for Multicopters to Avoid Non-Cooperative Moving Obstacles

Quan Quan, *Member, IEEE*, Rao Fu, and Kai-Yuan Cai

Abstract—Unmanned Aerial Vehicles (UAVs) are now becoming increasingly accessible to amateur and commercial users alike. The main task for UAVs is to keep a prescribed separation with obstacles in the air. In this paper, a collision-avoidance control method for non-cooperative moving obstacles is proposed for a multicopter with the altitude hold mode by using a Lyapunov-like barrier function. Lyapunov-like functions are designed elaborately, based on which formal analysis and proofs of the proposed control are made to show that the collision-avoidance control problem can be solved if the moving obstacle is slower than the multicopter. The result can be extended to some cases of multiple obstacles. What is more, by the proposed control, a multicopter can keep away from obstacles as soon as possible, once obstacles enter into the safety area of the multicopter accidentally, and converge to the waypoint. Simulations and experiments are given to show the effectiveness of the proposed method by showing the distance between UAV and waypoint, obstacles respectively.

Index Terms—UAV; swarm; collision avoidance; artificial potential; eVTOL; UTM.

I. INTRODUCTION

A. Background

Airspace is utilized today by far lesser aircraft than it can accommodate, especially low altitude airspace. There are more and more applications for UAVs in low altitude airspace, ranging from on-demand package delivery to traffic and wildlife surveillance, an inspection of infrastructure, search and rescue, agriculture, and cinematography. Air traffic for UAVs attracted more and more research [1],[2]. One of the chief concerns regarding UAVs is the possibility of collision [3],[4]. For such a purpose, a collision-avoidance scheme must present a feasible path for the UAV to take in order to maintain a minimum separation distance from obstacles in the air. Traditionally, the main role of air traffic management (ATM) is to keep a prescribed separation among all aircraft by using centralized control. However, it is infeasible for increasing UAVs because the traditional control method lacks scalability. In order to address such a problem, free flight is a developing air traffic control method that uses no centralized control [5],[6]. Free flight is very challenging in low altitude airspace because the environment is complex and dynamic. Namely, many obstacles are dense, moving [7], and unpredictable [8].

B. Existing Avoidance Techniques

The avoidance technique has been studied extensively [9],[10]. The close-range air avoidance algorithms can be

roughly divided into four categories [5]: trajectory-projection based method, online table based method, force field based method, and optimal trajectory method. A simulation study of four typical collision avoidance methods can be found in [11].

• Trajectory-Projection Based Method

The trajectory-based projection method needs to estimate the current state of the obstacle (such as position and velocity) and predict its trajectory. If the position of a UAV enters this dangerous area, a new heading angle command is immediately generated to cause the UAV to leave the dangerous area. After leaving the dangerous area, the UAV returns back to the original trajectory along with the original heading. The velocity obstacle method [12] is one of the classical methods. This method is simple, straightforward, and easy to implement. In [13], the collision avoidance problem was solved for multicopters by combining geometric constraints and kinematics equations. The maneuver generated from the selective velocity obstacle method can avoid obstacles while incorporating the right-of-way rules from the original route [14]. Furthermore, a three-dimensional extension of the velocity obstacle method can reactively generate an avoidance maneuver by changing the vehicle velocity vector based on the encounter geometry [15]. The trajectory projection method is more suitable for the control avoidance strategy based on the vision sensor or the fixed-wing aircraft maneuver. Because the visual sensor often only obtains the orientation of the obstacle and cannot measure the relative position, it is a relatively straightforward control method by changing the flight heading angle [10]. As for the fixed-wing aircraft, the change in direction is better to slowing down the speed.

• Online Table Based Method

Once the obstacles' status (location and speed) is received, this method will search its online form and determine the best way to maneuver. In [16], a robust and efficient algorithm was proposed based on decomposing a large multi-agent Markov decision process and integrating its solutions to generate recommendations for each aircraft. In [17], the concept of rapidly exploring random trees (RRT) originally investigated in [18] was used to find dynamically feasible obstacle-free paths. After obtaining an obstacle-free path, a path planner was used to avoid obstacles. When the environment is complex or local information is observed, the online table based method may fail or requires larger computation time to update frequently.

• Force Field Based Method

Force field based methods typically use attractive forces (maintaining on the original path or following the original destination) and repulsive forces (avoiding potential conflicts) to generate control commands for the next step. The weights of

Q. Quan, R. Fu and K.-Y. Cai are with the School of Automation Science and Electrical Engineering, Beihang University, Beijing 100191, China (e-mail: qq_buaa@buaa.edu.cn; buaafurao@buaa.edu.cn; kycai@buaa.edu.cn).

the different forces are adjusted online to balance the trade-offs between the different forces. In [19], a general and distributed air traffic control scheme using autonomous UAVs is proposed for dense traffic conditions, and 30 autonomous UAVs are used for verification in coordinated outdoor flight. In [20], the traffic simulation scene of dense multicopters in 2D and 3D open space was studied in the presence of a real environment of sensor noise, communication delay, limited communication range, limited sensor update rate, and limited power. One disadvantage of the force field based method is the risk of getting stuck in local minima [21].

• Optimal Trajectory Method

As for the optimal trajectory method, it uses optimization methods to plan feasible trajectories. In [22], the predictive control algorithm was used to calculate the optimal waypoint, which can avoid the static obstacles detected on the way while reaching the destination. In [23], a guidance method with obstacle avoidance capability was designed and analyzed to help the aircraft reach its destination quickly while avoiding collision with other aircraft. This method expressed the collision avoidance problem as a Markov decision process and solved it using the Monte Carlo tree search method. Based on approximate aircraft dynamics, a mixed-integer linear programming approach was used to create flight paths without collisions [24],[25]. A real-time path planning algorithm was proposed for UAVs to avoid collisions with other aircraft [26]. The reachable set was used to represent the set of possible trajectories of the obstacle aircraft and was used for collision prediction in UAV path planning. The optimal trajectory method is very suited for known static obstacles. As for moving obstacle avoidance, the optimal trajectory method requires to predict the motion of moving obstacles. What is more, this method requires a larger computation time to update frequently.

C. Proposed Force Field Method

As for our problem, the force field method possesses a number of distinct advantages when compared to other methods [21],[27]. First, it uses a simple formula to react to obstacles as they appear, which have low demand for computing resources, making them very suitable for real-time avoidance. It can work on a processor with limited processing capabilities. Moreover, this method can distribute onto each UAV. If the UAV has an active detection device, then these UAVs need not communicate with each other.

In this paper, a force field method is proposed for multicopters to avoid multiple moving obstacles by using a Lyapunov-like barrier function. Because of the larger uncertainties, the problem for multicopters in the air differs from those for some indoor robots with a highly accurate position estimation and control. The conflict of an obstacle and a multicopter is often defined that their distance is less than a safety distance. However, the conflict will happen in practice even if conflict avoidance is proved formally because some assumptions will be violated in practice. Even though the multicopters may not have a real collision in physics because the safety distance is often set largely by considering

uncertainties. In most literature, if their distance is less than a safety distance, then their control schemes either do not work or even push the agent towards the center of the safety area rather than the outside of the safety area. For example, some studies have used the following barrier function terms for collision avoidance, such as $1/(\|\mathbf{p}_i - \mathbf{p}_j\| - R)$ [28] or $\ln(\|\mathbf{p}_i - \mathbf{p}_j\| - R)$ [29], where \mathbf{p}_i , \mathbf{p}_j are two multicopters' positions, and $R > 0$ is the separation distance. The principle is to design a controller to make the barrier function terms bounded so that $\|\mathbf{p}_i - \mathbf{p}_j\| > R$ if $\|\mathbf{p}_i(0) - \mathbf{p}_j(0)\| > R$. Otherwise, $\|\mathbf{p}_i - \mathbf{p}_j\| = R$ will make the barrier function term unbounded. The separation distance for robots indoor is often the sum of the two robots' physical radius, namely $\|\mathbf{p}_i - \mathbf{p}_j\| < R$ will not happen in practice. But, the separation distance is set largely for multicopters compared with their sizes. Due to some uncertainties such as communication delay, $\|\mathbf{p}_i - \mathbf{p}_j\| < R$ will happen in the air. As a consequence, the control corresponding to the barrier function terms mentioned above will make $\|\mathbf{p}_i - \mathbf{p}_j\| \rightarrow 0$ if $1/(\|\mathbf{p}_i - \mathbf{p}_j\| - R)$ is used (the two multicopters are pushed together by the designed controller) or appear numerical computation error if $\ln(\|\mathbf{p}_i - \mathbf{p}_j\| - R)$ is used.

D. Contributions

In view of this, a practical controller is proposed to solve the moving non-cooperative obstacle avoidance problem, where the non-cooperative obstacle is that will not make avoidance with the multicopter. Compared with cooperative obstacles, the non-cooperative obstacle is more difficult to deal with. Since the multicopter's speed is confined, it cannot avoid some non-cooperative (hostile) moving obstacles such as a fast bullet. However, cooperative obstacles and the multicopter can make avoidance with each other by slowing speed or changing their directions simultaneously [30]. On the other hand, when obstacles are moving, the convergence analysis is difficult because the resulting equilibriums maybe not constant anymore, which are not easy to determine and analyze. This is different from the analysis of static obstacles. For this, in this paper, the instability about angle rather than position is proved for the case that the multicopter is in front of an obstacle moving direction. With this result, the convergence analysis is proved for one moving obstacle avoidance control problem. Furthermore, one moving obstacle avoidance control extends to two types of multiple moving obstacle avoidance control problems. The contributions lie in the practicability and properties of this method. The practicability of the proposed control lies in the following two features: (i) a double integral model with the given velocity command as input is proposed for multicopters, where the maneuverability has been taken into consideration; (ii) the maximum velocity command in the proposed distributed controller is confined. With the two features, the properties of the proposed method lie in the following two features: (i) formal proofs about conflict avoidance for one moving obstacle problem are given; (ii) formal proofs about the convergence to the desired waypoints are further given.

II. PROBLEM FORMULATION

In this section, a multicopter control model and an obstacle model are introduced first, including two types of areas, namely safety area and avoidance area, used for control. Then, the obstacle avoidance control problem is formulated.

A. Control Model

1) *Multicopter Control Model*: Many organizations or companies have designed some open-source semi-autonomous autopilots or offered semi-autonomous autopilots with Software Development Kits. The semi-autonomous autopilots can be used for velocity control of multicopters. For example, A3 autopilots released by DJI allow the range of the horizontal velocity command from $-10\text{m/s} \sim 10\text{m/s}$ [31]. With such an autopilot, the velocity of a multicopter can track a given velocity command in a reasonable time. Not only can this avoid the trouble of modifying the low-level source code of autopilots, but also it can utilize commercial autopilots to complete various tasks. Based on this, we suppose that there is a multicopter with the altitude hold mode in local airspace satisfying the following model

$$\begin{aligned}\dot{\mathbf{p}} &= \mathbf{v} \\ \dot{\mathbf{v}} &= -l(\mathbf{v} - \mathbf{v}_c)\end{aligned}\quad (1)$$

where $l > 0$, $\mathbf{p} \in \mathbb{R}^2$ and $\mathbf{v} \in \mathbb{R}^2$ are the position and velocity of the multicopter, $\mathbf{v}_c \in \mathbb{R}^2$ is the velocity command of the multicopter. The control gain l depends on the multicopter and the semi-autonomous autopilot used, which can be obtained through flight experiments. From the model (1), $\lim_{t \rightarrow \infty} \|\mathbf{v}(t) - \mathbf{v}_c\| = 0$ if \mathbf{v}_c is constant. Here, the velocity command \mathbf{v}_c for the multicopter is subject to a saturation defined as

$$\text{sat}(\mathbf{v}, v_m) \triangleq \begin{cases} \mathbf{v} & \|\mathbf{v}\| \leq v_m \\ v_m \frac{\mathbf{v}}{\|\mathbf{v}\|} & \|\mathbf{v}\| > v_m \end{cases} \quad (2)$$

where $v_m > 0$ is the setting maximum speed of the multicopter, $\mathbf{v} \triangleq [v_1 \ v_2]^T \in \mathbb{R}^2$. This implies

$$\|\mathbf{v}_c\| \leq v_m. \quad (3)$$

The saturation function $\text{sat}(\mathbf{v}, v_m)$ and the vector \mathbf{v} are parallel all the time so the multicopter can keep the flying direction the same if $\|\mathbf{v}\| > v_m$ [28]. The saturation function can be rewritten as

$$\text{sat}(\mathbf{v}, v_m) = \kappa_{v_m}(\mathbf{v}) \mathbf{v}$$

where

$$\kappa_{v_m}(\mathbf{v}) \triangleq \begin{cases} 1, & \|\mathbf{v}\| \leq v_m \\ \frac{v_m}{\|\mathbf{v}\|}, & \|\mathbf{v}\| > v_m \end{cases}.$$

It is obvious that $0 < \kappa_{v_m}(\mathbf{v}) \leq 1$. Sometimes, $\kappa_{v_m}(\mathbf{v})$ will be written as κ_{v_m} for short. According to this, if and only if $\mathbf{v} = \mathbf{0}$, then

$$\mathbf{v}^T \text{sat}(\mathbf{v}, v_m) = 0.$$

In the presence of the saturation constraint, the velocity is confined no matter how the controller is designed.

Proposition 1. If $\|\mathbf{v}(0)\| \leq v_m$ and the model (1) is subject to (2), namely

$$\begin{aligned}\dot{\mathbf{p}} &= \mathbf{v} \\ \dot{\mathbf{v}} &= -l(\mathbf{v} - \text{sat}(\mathbf{v}_c, v_m))\end{aligned}$$

then $\|\mathbf{v}(t)\| \leq v_m$, $t \geq 0$.

Proof. See Appendix. \square

Remark 1. Because the propellers often provide the unidirectional upward thrust, the descending and climbing ability of a multicopter are different, the model (1) is not very suit for the altitude control. So, here, we only consider a multicopter with the altitude hold mode in 2D space for simplicity. When a Vertical TakeOff and Landing (VTOL) UAV takes flight with the altitude hold mode, the model (1) can be adopted.

2) *Obstacle Model*: In the same local airspace, there exists a moving obstacle (it may be an aircraft or a balloon) defined as

$$\mathcal{O} = \{\mathbf{x} \in \mathbb{R}^2 \mid \|\mathbf{x} - \mathbf{p}_o\| < r_o\}$$

where $r_o > 0$ is the obstacle radius, and $\mathbf{p}_o \in \mathbb{R}^2$ is the center of mass of the obstacle. Define

$$\boldsymbol{\xi}_o \triangleq \mathbf{p}_o + \frac{1}{l} \mathbf{v}_o$$

where $\mathbf{v}_o \in \mathbb{R}^2$ is the velocity of the obstacle. The obstacle satisfies the following model

$$\max \|\dot{\boldsymbol{\xi}}_o\| \leq v_o$$

where $v_o > 0$. This is a general model for any obstacle with bounded velocity and acceleration. Let

$$\dot{\boldsymbol{\xi}}_o = \mathbf{a}_o. \quad (4)$$

with $\max \|\mathbf{a}_o\| \leq v_o$. Then (4) can be rewritten as

$$\begin{aligned}\dot{\mathbf{p}}_o &= \mathbf{v}_o \\ \dot{\mathbf{v}}_o &= -l(\mathbf{v}_o - \mathbf{a}_o).\end{aligned} \quad (5)$$

In particular, if $\|\mathbf{v}_o(0)\| \leq v_o$ and $\mathbf{a}_o = \mathbf{v}_o(0)$, then the obstacle is moving with a constant velocity. If $\mathbf{v}_o = \mathbf{0}$, then the obstacle is static.

3) *Filtered Position Model*: As shown in Fig. 1, although the position distances of the three cases are the same, namely a marginal avoidance distance, the case in Fig. 1(b) needs to carry out avoidance urgently by considering the velocity. However, the case in Fig. 1(a) in fact does not need to be considered.

With such an intuition, a filtered position is defined as follows:

$$\boldsymbol{\xi} \triangleq \mathbf{p} + \frac{1}{l} \mathbf{v}. \quad (6)$$

Then

$$\begin{aligned}\dot{\boldsymbol{\xi}} &= \dot{\mathbf{p}} + \frac{1}{l} \dot{\mathbf{v}} \\ &= \mathbf{v} - \frac{1}{l} l(\mathbf{v} - \mathbf{v}_c) \\ &= \mathbf{v}_c.\end{aligned} \quad (7)$$

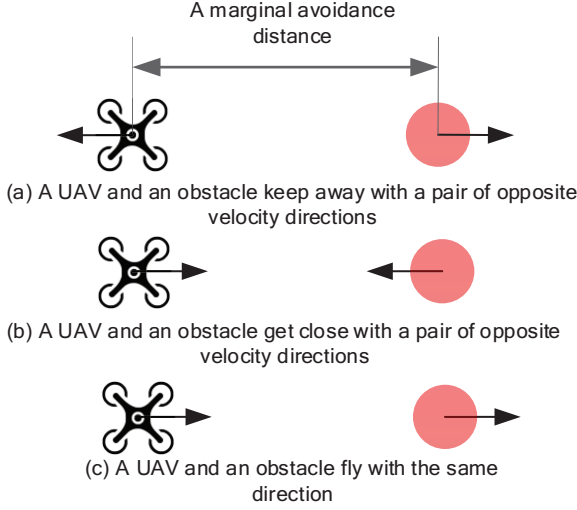


Fig. 1. Intuitive interpretation for filtered position.

Define

$$\begin{aligned}\tilde{\mathbf{p}}_o &\triangleq \mathbf{p} - \mathbf{p}_o \\ \tilde{\mathbf{v}}_o &\triangleq \mathbf{v} - \mathbf{v}_o \\ \tilde{\boldsymbol{\xi}}_o &\triangleq \tilde{\mathbf{p}}_o + \frac{1}{l} \tilde{\mathbf{v}}_o\end{aligned}\quad (8)$$

and

$$r_v = \frac{v_m + v_o}{l}. \quad (9)$$

According to *Proposition 1*, we have

$$\frac{1}{l} \|\tilde{\mathbf{v}}_o\| \leq r_v. \quad (10)$$

In the following, a relationship between the position error and the filtered position error is shown.

Proposition 2. For the multicopter and the obstacle, *if and only if* the filtered position error satisfies

$$\|\tilde{\boldsymbol{\xi}}_o(t)\| \geq \sqrt{r^2 + r_v^2}, \quad (11)$$

and $\|\tilde{\mathbf{p}}_o(0)\| \geq r$, then $\|\tilde{\mathbf{p}}_o(t)\| \geq r$, where $t > 0$. The relationship “=” holds if $\frac{\mathbf{v}_o^T \tilde{\mathbf{v}}_o}{\|\mathbf{v}_o\| \|\tilde{\mathbf{v}}_o\|} = -1$. Furthermore, if $\|\tilde{\boldsymbol{\xi}}_o(t)\| > \sqrt{r^2 + r_v^2}$ and $\|\tilde{\mathbf{p}}_o(0)\| > r$, then $\|\tilde{\mathbf{p}}_o(t)\| > r$, where $t > 0$.

Proof. See Appendix. \square

B. Two Types of Areas around a Multicopter

Two types of areas used for control, namely *safety area* and *avoidance area*, are introduced.

1) *Safety Area*: In order to avoid a conflict, as shown in Figure 2, the *safety area* of a multicopter is defined as

$$\mathcal{S} = \{\mathbf{x} \in \mathbb{R}^2 \mid \|\mathbf{x} - \boldsymbol{\xi}\| \leq r_s\} \quad (12)$$

where $r_s > 0$ is the safety radius. It should be noted that we consider the velocity of the multicopter in the definition of \mathcal{S} . For the multicopter, no *conflict* with the obstacle implies

$$\mathcal{S} \cap \mathcal{O} = \emptyset$$

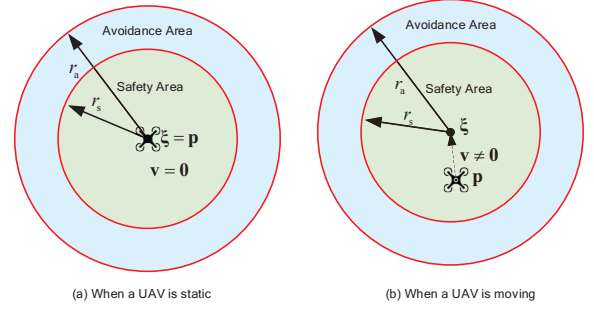


Fig. 2. Safety area and avoidance area of a UAV.

namely

$$\|\tilde{\boldsymbol{\xi}}_o\| > r_s + r_o. \quad (13)$$

Proposition 2 implies that the multicopter and the obstacle will be separated largely enough if (13) is satisfied with a safety radius r_s large enough.

2) *Avoidance Area*: Besides the safety area, there exists an *avoidance area* used for starting avoidance control. If the obstacle is out of the avoidance area of the multicopter, then the obstacle will not need to be avoided. For the multicopter, the *avoidance area* for other multicopters is defined as

$$\mathcal{A} = \{\mathbf{x} \in \mathbb{R}^2 \mid \|\mathbf{x} - \boldsymbol{\xi}\| \leq r_a\} \quad (14)$$

where $r_a > 0$ is the *avoidance radius*. It should be noted that we consider the velocity of the multicopter in the definition of \mathcal{A} . If

$$\mathcal{A} \cap \mathcal{O} \neq \emptyset,$$

namely

$$\|\tilde{\boldsymbol{\xi}}_o\| \leq r_a$$

then the obstacle should be avoided by the multicopter. When the obstacle just enters into the avoidance area of the multicopter, it is required that they have not conflicted at the beginning. Therefore, we require

$$r_a > r_s.$$

C. Moving Obstacle Avoidance Control Problem

Before introducing the problem, the following assumptions are imposed.

Assumption 1. The information of obstacle \mathcal{O} can be detected, where the velocity of the obstacle \mathbf{v}_o is constant.

Assumption 2. The multicopter's initial filtered position error $\tilde{\boldsymbol{\xi}}_o(0) \in \mathbb{R}^2$ satisfies

$$\|\tilde{\boldsymbol{\xi}}_o(0)\| > r_s + r_o$$

and $\|\mathbf{v}(0)\| \leq v_m$.

Assumption 3. The goal waypoint is static. Furthermore, if the obstacle is static, then

$$\|\mathbf{p}_{wp} - \mathbf{p}_o\| \geq r_a + r_o.$$

Based on *Assumptions 1-3*, we have the *moving obstacle avoidance control problem* stated in the following.

Moving Obstacle Avoidance Control Problem. Let $\mathbf{p} \in \mathbb{R}^2$ be the position of the multicopter, and $\mathbf{p}_{wp} \in \mathbb{R}^2$ be the goal waypoint. Under *Assumptions 1-3*, design the velocity input \mathbf{v}_c for the multicopter modeled in (1) to guide it flying until it arrives at the goal waypoint \mathbf{p}_{wp} , meanwhile avoiding colliding the obstacle \mathcal{O} . The one moving obstacle avoidance control problem will be extended for the multiple moving obstacles avoidance control problem.

Remark 2. With the help of surveillance systems on the ground or detection devices onboard (cameras or radars), the information of obstacle \mathcal{O} can be detected. The assumption about the constant obstacle velocity is only for the convenience of the convergence proof to the waypoint. As pointed by the following *Lemma 2*, the collision-avoidance control problem can be solved if the moving obstacle is slower than the multicopter with only *Assumption 2*. *Assumptions 2-3* imply that the multicopter and its waypoint are not close to the obstacle too much initially. As for *Assumption 3*, if $r_a = 3\text{m}$, it only requires that the waypoint keeps away from the obstacle 3m. It is reasonable in practice.

III. PRELIMINARIES

A. Line Integral Lyapunov Function

In the following, we will design a new type of Lyapunov Functions, called *Line Integral Lyapunov Function*. This type of Lyapunov functions is inspired by its scalar form [32, p.74]. If $xf(x) > 0$ for $x \neq 0$, then $V'_i(y) = \int_0^y f(x)dx > 0$ when $y \neq 0$. The derivative is $\dot{V}'_i = f(y)\dot{y}$. A line integral Lyapunov function for vectors is defined as

$$V_{li}(\mathbf{y}) = \int_{C_y} \text{sat}(\mathbf{x}, a)^T d\mathbf{x} \quad (15)$$

where $a > 0$, $\mathbf{x} \in \mathbb{R}^n$, C_y is a line from $\mathbf{0}$ to $\mathbf{y} \in \mathbb{R}^n$. In the following lemma, we will show its properties.

Lemma 1. Suppose that the line integral Lyapunov function V_{li} is defined as (15). Then (i) $V_{li}(\mathbf{y}) > 0$ if $\|\mathbf{y}\| \neq 0$; (ii) if $\|\mathbf{y}\| \rightarrow \infty$, then $V_{li}(\mathbf{y}) \rightarrow \infty$; (iii) if $V_{li}(\mathbf{y})$ is bounded, then $\|\mathbf{y}\|$ is bounded.

Proof. Since

$$\text{sat}(\mathbf{x}, a) = \kappa_a(\mathbf{x}) \mathbf{x}$$

the function (15) can be written as

$$V_{li}(\mathbf{y}) = \int_{C_y} \kappa_a(\mathbf{x}) \mathbf{x}^T d\mathbf{x} \quad (16)$$

where

$$\kappa_a(\mathbf{x}) \triangleq \begin{cases} 1, & \|\mathbf{x}\| \leq a \\ \frac{a}{\|\mathbf{x}\|}, & \|\mathbf{x}\| > a \end{cases}.$$

Let $z = \|\mathbf{x}\|$. Then the function (16) becomes

$$\begin{aligned} V_{li}(\mathbf{y}) &= \int_{C_y} \frac{\kappa_a(\mathbf{x})}{2} dz^2 \\ &= \int_0^{\|\mathbf{y}\|} \kappa_a(\mathbf{x}) z dz. \end{aligned}$$

- If $\|\mathbf{y}\| \leq a$, then $\kappa_a(\mathbf{x}) = 1$. Consequently,

$$V_{li}(\mathbf{y}) = \frac{1}{2} \|\mathbf{y}\|^2. \quad (17)$$

- If $\|\mathbf{y}\| > a$, then

$$\int_0^{\|\mathbf{y}\|} \kappa_a(\mathbf{x}) z dz = \int_0^a z dz + \int_a^{\|\mathbf{y}\|} \frac{a}{\|\mathbf{x}\|} z dz.$$

Since $z = \|\mathbf{x}\|$, we have

$$V_{li}(\mathbf{y}) = \frac{1}{2} a^2 + a(\|\mathbf{y}\| - a). \quad (18)$$

Therefore, from the form of (17) and (18), we have (i) $V_{li}(\mathbf{y}) > 0$ if $\|\mathbf{y}\| \neq 0$. (ii) if $\|\mathbf{y}\| \rightarrow \infty$, then $V_{li}(\mathbf{y}) \rightarrow \infty$; (iii) if $V_{li}(\mathbf{y})$ is bounded, then $\|\mathbf{y}\|$ is bounded. \square

B. Two Smooth Functions

Two smooth functions are defined for the following Lyapunov-like function design. As shown in Figure 3(a), define a second-order differentiable ‘bump’ function as [29]

$$\sigma(x, d_1, d_2) = \begin{cases} 1 & \text{if } x \leq d_1 \\ Ax^3 + Bx^2 + Cx + D & \text{if } d_1 \leq x \leq d_2 \\ 0 & \text{if } d_2 \leq x \end{cases} \quad (19)$$

with $A = -2/(d_1 - d_2)^3$, $B = 3(d_1 + d_2)/(d_1 - d_2)^3$, $C = -6d_1d_2/(d_1 - d_2)^3$ and $D = d_2^2(3d_1 - d_2)/(d_1 - d_2)^3$. The derivative of $\sigma(x, d_1, d_2)$ with respect to x is

$$\frac{\partial \sigma(x, d_1, d_2)}{\partial x} = \begin{cases} 0 & \text{if } x \leq d_1 \\ 3Ax^2 + 2Bx + C & \text{if } d_1 \leq x \leq d_2 \\ 0 & \text{if } d_2 \leq x \end{cases}.$$

Define another smooth function as shown in Figure 3(b) to approximate a saturation function

$$\bar{s}(x) = \min(x, 1), x \geq 0$$

that

$$s(x, \epsilon_s) = \begin{cases} x & 0 \leq x \leq x_1 \\ (1 - \epsilon_s) + \sqrt{\epsilon_s^2 - (x - x_2)^2} & x_1 \leq x \leq x_2 \\ 1 & x_2 \leq x \end{cases} \quad (20)$$

with $x_2 = 1 + \frac{1}{\tan 67.5^\circ} \epsilon_s$ and $x_1 = x_2 - \sin 45^\circ \epsilon_s$. Since it is required $x_1 \geq 0$, one has $\epsilon_s \leq \frac{\tan 67.5^\circ}{\tan 67.5^\circ \sin 45^\circ - 1}$. For any $\epsilon_s \in [0, \frac{\tan 67.5^\circ}{\tan 67.5^\circ \sin 45^\circ - 1}]$, it is easy to see

$$s(x, \epsilon_s) \leq \bar{s}(x) \quad (21)$$

and

$$\limsup_{\epsilon_s \rightarrow 0} \sup_{x \geq 0} |\bar{s}(x) - s(x, \epsilon_s)| = 0. \quad (22)$$

The derivative of $s(x, \epsilon_s)$ with respect to x is

$$\frac{\partial s(x, \epsilon_s)}{\partial x} = \begin{cases} 1 & 0 \leq x \leq x_1 \\ \frac{x_2 - x}{\sqrt{\epsilon_s^2 - (x - x_2)^2}} & x_1 \leq x \leq x_2 \\ 0 & x_2 \leq x \end{cases}.$$

For any $\epsilon_s > 0$, we have $\sup_{x \geq 0} |\partial s(x, \epsilon_s) / \partial x| \leq 1$.

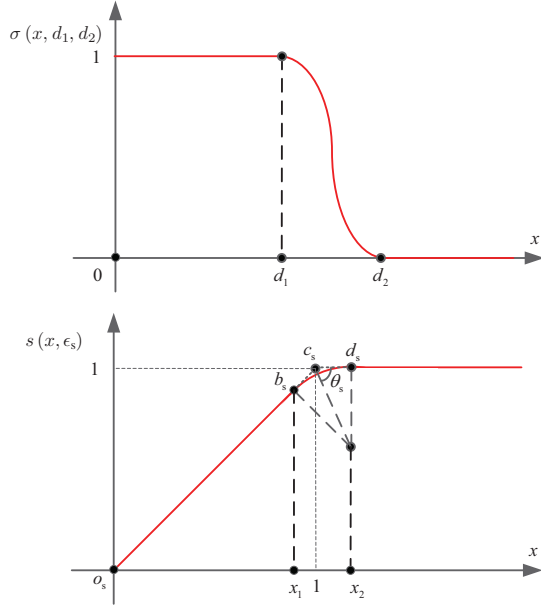


Fig. 3. Two smooth functions. For a smooth saturation function, $\theta_s = 67.5^\circ$.

IV. OBSTACLE AVOIDANCE CONTROL

The idea of the proposed method is similar to that of the artificial potential field (APF) method. In this method, the airspace is formulated as an APF. For a given multicopter, only is the corresponding waypoint assigned *attractive potential*, while the obstacle is assigned *repulsive potentials*. A multicopter in the field will be attracted to the waypoint, while being repelled by the obstacle.

A. Error Model

Define position error as

$$\tilde{\mathbf{p}}_{\text{wp}} \triangleq \mathbf{p} - \mathbf{p}_{\text{wp}}$$

and the filtered position error as

$$\tilde{\xi}_{\text{wp}} \triangleq \xi - \mathbf{p}_{\text{wp}}.$$

By (5) and (7), the derivative of the filtered errors are

$$\dot{\tilde{\xi}}_{\text{wp}} = \mathbf{v}_c \quad (23)$$

$$\dot{\tilde{\xi}}_o = \mathbf{v}_c - \mathbf{a}_o. \quad (24)$$

B. Lyapunov-Like Function Design and Analysis

Define a smooth curve $C_{\tilde{\xi}_{\text{wp}}}$ from $\mathbf{0}$ to $\tilde{\xi}_{\text{wp}}$. Then, the line integral of $\text{sat}(\tilde{\xi}_{\text{wp}}, v_m)$ along $C_{\tilde{\xi}_{\text{wp}}}$ is

$$V_w(\tilde{\xi}_{\text{wp}}) = \int_{C_{\tilde{\xi}_{\text{wp}}}} \text{sat}(k_1 \mathbf{x}, v_m)^T d\mathbf{x} \quad (25)$$

where $k_1 > 0$. From the definition and Lemma 1, $V_w \geq 0$. With the two defined functions (19) and (20), a Lyapunov-like function is defined as

$$V_o(\|\tilde{\xi}_o\|) = \frac{k_2 \sigma_o(\|\tilde{\xi}_o\|)}{(1 + \epsilon) \|\tilde{\xi}_o\| - (\gamma r_s + r_o) s\left(\frac{\|\tilde{\xi}_o\|}{\gamma r_s + r_o}, \epsilon_s\right)} \quad (26)$$

where $k_2, \epsilon_s > 0$, $\gamma > 1$, and $\sigma_o(x) \triangleq \sigma(x, \gamma r_s + r_o, r_a)$. The function V_o has the following properties:

- Property (i). $\partial V_o / \partial \|\tilde{\xi}_o\| \leq 0$ as V_o is a nonincreasing function with respect to $\|\tilde{\xi}_o\|$;
- Property (ii). if $\|\tilde{\xi}_o\| \geq r_a$, namely the obstacle is out of the avoidance area of the multicopter, then $\sigma_o(\|\tilde{\xi}_o\|) = 0$; consequently, $V_o = 0$ and $\partial V_o / \partial \|\tilde{\xi}_o\| = 0$; on the other hand, if $V_o = 0$, then $\|\tilde{\xi}_o\| \geq r_a$;
- Property (iii). if $0 < \|\tilde{\xi}_o\| < \gamma r_s + r_o$, namely the safety area of the multicopter and the obstacle area are close or have an intersection, then

$$\sigma_o(\|\tilde{\xi}_o\|) = 1$$

and there exists a sufficiently small $\epsilon_s > 0$ such that

$$s\left(\frac{\|\tilde{\xi}_o\|}{\gamma r_s + r_o}, \epsilon_s\right) \approx \frac{\|\tilde{\xi}_o\|}{\gamma r_s + r_o} < 1.$$

As a result,

$$V_o \approx \frac{k_2}{\epsilon \|\tilde{\xi}_o\|} > \frac{k_2}{\epsilon (\gamma r_s + r_o)} \quad (27)$$

which is very large as $\epsilon > 0$ is chosen very small.

The objective of the designed velocity command is to make $V_w(\tilde{\xi}_{\text{wp}})$ and $V_o(\|\tilde{\xi}_o\|)$ be zero or as small as possible. According to Lemma 1 and Property (ii), this implies $\|\tilde{\xi}_{\text{wp}}\| \rightarrow 0$ and $\|\tilde{\xi}_o\| \geq r_a$. Namely, the multicopter will arrive at the goal waypoint \mathbf{p}_{wp} and does not collide with the obstacle.

C. Controller Design

The velocity command for the multicopter modeled in (1) is designed as

$$\mathbf{v}_c = -\text{sat}\left(\text{sat}\left(k_1 \tilde{\xi}_{\text{wp}}, v_m\right) - a_o \tilde{\xi}_o, v_m\right) \quad (28)$$

where $k_1 > 0$ and¹

$$a_o = -\frac{\partial V_o}{\partial \|\tilde{\xi}_o\|} \frac{1}{\|\tilde{\xi}_o\|}. \quad (29)$$

Remark 3. The saturation constraint term $\text{sat}(k_1 \tilde{\xi}_{\text{wp}}, v_m)$ in (28) is very necessary. Without the saturation, the velocity command (28) becomes

$$\mathbf{v}_c = -\text{sat}\left(k_1 \tilde{\xi}_{\text{wp}} - a_o \tilde{\xi}_o, v_m\right).$$

¹ $a_o \geq 0$ according to the property (i) of V_o .

In this case, if the initial value $\tilde{\xi}_{wp}(0)$ is very large, then the term $k_1 \tilde{\xi}_{wp}$ will dominate until the multicopter is very close to the obstacle so that $a_o \tilde{\xi}_o$ can dominate. In this case, $a_o \approx \frac{k_2}{\epsilon} \frac{1}{\|\tilde{\xi}_o\|^3}$, which will increase sharply when the multicopter is very close to the obstacle. At that time, the multicopter will start to change the velocity to avoid a conflict. In practice, it may be too late by taking various uncertainties into consideration. The use of the maximum speeds v_m in the term $\text{sat}(k_1 \tilde{\xi}_{wp}, v_m)$ of the velocity command (28) will avoid such a danger.

Remark 4. The controller (28) can be written as a proportional (P) controller as

$$\mathbf{v}_c = \mathbf{p}_d - \mathbf{p}$$

where

$$\mathbf{p}_d = \mathbf{p} - \text{sat}\left(\text{sat}\left(k_1 \tilde{\xi}_{wp}, v_m\right) - a_o \tilde{\xi}_o, v_m\right). \quad (30)$$

In order to figure out the physical meaning of \mathbf{p}_d , suppose that $\mathbf{v} = \mathbf{0}$, $\mathbf{v}_o = \mathbf{0}$ and \mathbf{p} is close to the obstacle, namely $\|\mathbf{p} - \mathbf{p}_o\| < r_a$. This implies $a_o \tilde{\mathbf{p}}_o \neq \mathbf{0}$ according to the property of V_o . Then (30) becomes

$$\mathbf{p}_d = \mathbf{p} - \text{sat}\left(\text{sat}\left(k_1 \tilde{\mathbf{p}}_{wp}, v_m\right) - a_o \tilde{\mathbf{p}}_o, v_m\right). \quad (31)$$

Furthermore, let

$$k_1 = k_2 = 1.$$

Then \mathbf{p}_d has a concise form

$$\mathbf{p}_d = \mathbf{p} + \text{sat}(\mathbf{p}'_d, v_m)$$

where $\mathbf{p}'_d = \mathbf{p}'_{wp} + a_o(\mathbf{p} - \mathbf{p}_o)$ and $\mathbf{p}'_{wp} = \text{sat}(\mathbf{p}_{wp} - \mathbf{p}, v_m)$. The physical meaning of \mathbf{p}_d and \mathbf{p}'_d is shown in Figure 4. As shown, the contribution $\mathbf{p}_{wp} - \mathbf{p}$ is saturated by the term $\text{sat}(\mathbf{p}_{wp} - \mathbf{p}, v_m)$. Otherwise, \mathbf{p}_d will still point to the obstacle until the multicopter is very close to the obstacle.

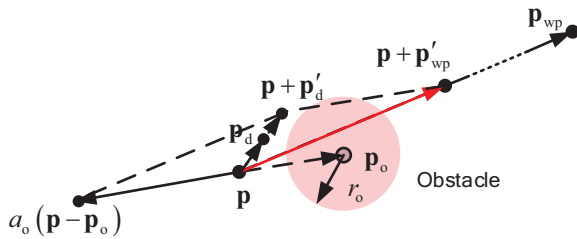


Fig. 4. Desired position generated for obstacle avoidance.

Remark 5. Although the property of the obstacle avoidance is proved, the case such as $\|\tilde{\xi}_o\| < r_s + r_o$ may still happen in practice due to unpredictable uncertainties. For example, the obstacle cannot be detected until it is very close to the multicopter. However, this may not imply that the multicopter has a collision with the obstacle physically. In this case,

$$a_o \approx \frac{k_2}{\epsilon} \frac{1}{\|\tilde{\xi}_o\|^3}.$$

Since ϵ is chosen to be sufficiently small, the term $a_o \tilde{\xi}_o$ will dominate so that the velocity command \mathbf{v}_c becomes

$$\mathbf{v}_c \approx \text{sat}\left(\frac{k_2}{\epsilon} \frac{1}{\|\tilde{\xi}_o\|^2} \frac{\tilde{\xi}_o}{\|\tilde{\xi}_o\|}, v_m\right).$$

This implies that, by recalling (24), $\|\tilde{\xi}_o\|$ will be increased fast with its maximum speed. This implies that the multicopter will keep away from the obstacle immediately.

D. Stability Analysis

In order to investigate the convergence to the goal waypoint and the obstacle avoidance behaviour, a function is defined as follows

$$V_1 = V_w + V_o \quad (32)$$

where V_w is defined in (25), and V_o is defined in (26). Before introducing the main result, three lemmas are needed.

Lemma 2. Under *Assumption 2*, for (1), if the velocity input \mathbf{v}_c is designed as in (28) and $v_m > v_o$, then there exist sufficiently small $\epsilon, \epsilon_s > 0$ and any $\gamma > 1$ in a_0 such that $\|\tilde{\xi}_o(t)\| > r_s + r_o, t \in [0, \infty)$.

Proof. See Appendix. \square

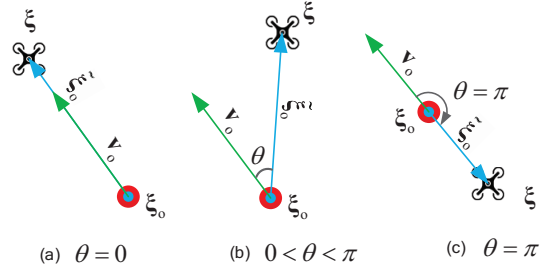


Fig. 5. Relationship between filtered position error and the velocity of the obstacle.

As shown in Figure 5, let

$$\cos \theta = \frac{\tilde{\xi}_o^T \mathbf{v}_o}{\|\mathbf{v}_o\| \|\tilde{\xi}_o\|} \quad (33)$$

where $\theta \in [0, \pi]$ is the angle between $\tilde{\xi}_o$ and \mathbf{v}_o . The positive direction of the rotation is clockwise without loss of generality. The next lemma is to show that the relationship between the obstacle and the multicopter will tend to the case shown in Figure 5(c).

Lemma 3. Under *Assumptions 1-3*, for (1), if the velocity input \mathbf{v}_c is designed as in (28) and $\mathbf{v}_o \neq \mathbf{0}$, then $\lim_{t \rightarrow \infty} \theta(t) = \pi$ for almost all $\tilde{\xi}_o(0)$.

Proof. See Appendix. \square

Lemma 4. If $0 < \rho \mathbf{I}_n < \Lambda = \Lambda^T \in \mathbb{R}^{n \times n}$ is a symmetric positive-definite matrix, and $\mathbf{X} \in \mathbb{R}^{n \times n}$ is a symmetric matrix with $\text{rank}(\mathbf{X}) \leq n - 1$, then $\lambda_{\max}(\Lambda + \mathbf{X}) > \rho > 0$, where $\lambda_{\max}(\Lambda + \mathbf{X})$ denotes the maximum eigenvalue of $\Lambda + \mathbf{X}$.

Proof. See Appendix. \square

With *Lemmas 1-4* in hand, we can state the main result.

Theorem 1. Under *Assumptions 1-3*, suppose that the velocity input for the multicopter is designed as in (28). Then there exist sufficiently small $\epsilon, \epsilon_s > 0$ and $\gamma > 1$ in a_0 such that $\lim_{t \rightarrow \infty} \|\tilde{\mathbf{p}}_{wp}(t)\| = 0$ and $\|\tilde{\boldsymbol{\xi}}_o(t)\| > r_s + r_o, t \in [0, \infty)$ for almost² all $\tilde{\boldsymbol{\xi}}_{wp}(0)$ when $v_m > v_o$.

Proof. By *Lemma 2*, there exist sufficiently small $\epsilon, \epsilon_s > 0$ and any $\gamma > 1$ in a_0 such that $\|\tilde{\boldsymbol{\xi}}_o(t)\| > r_s + r_o, t \in [0, \infty)$, namely the obstacle avoidance can be achieved. In order to investigate the convergence to the goal waypoint, a function is defined as in (32). According to the line integrals of vector fields[33, p. 911], one has

$$V_1 = \int_0^t \text{sat} \left(k_1 \tilde{\boldsymbol{\xi}}_{wp}, v_m \right)^T \dot{\tilde{\boldsymbol{\xi}}}_{wp} d\tau + V_o.$$

The derivative of V_1 along the solution to (23) and (24) is

$$\dot{V}_1 = \left(\text{sat} \left(k_1 \tilde{\boldsymbol{\xi}}_{wp}, v_m \right) - a_o \tilde{\boldsymbol{\xi}}_o \right)^T \mathbf{v}_c + a_o \tilde{\boldsymbol{\xi}}_o^T \mathbf{v}_o$$

where a_o are defined in (29) and $\mathbf{a}_o = \mathbf{v}_o$ according to *Assumption 1*. By using the velocity input (28), \dot{V}_1 becomes

$$\begin{aligned} \dot{V}_1 = & - \left(\text{sat} \left(k_1 \tilde{\boldsymbol{\xi}}_{wp}, v_m \right) - a_o \tilde{\boldsymbol{\xi}}_o \right)^T \\ & \cdot \text{sat} \left(\text{sat} \left(k_1 \tilde{\boldsymbol{\xi}}_{wp}, v_m \right) - a_o \tilde{\boldsymbol{\xi}}_o, v_m \right) + a_o \tilde{\boldsymbol{\xi}}_o^T \mathbf{v}_o. \end{aligned} \quad (34)$$

In the following, we will discuss the stability of two cases, namely $\mathbf{v}_o = \mathbf{0}$ and $\mathbf{v}_o \neq \mathbf{0}$.

- **Property of function V_1 .** Before applying *invariant set theorem* [32], we will study the property of function V_1 . Let $\Omega = \{ \boldsymbol{\xi} \mid V_1(\boldsymbol{\xi}) \leq l_0 \}$, $l_0 > 0$. According to *Lemma 2*, $V_o > 0$. Therefore, $V_1(\boldsymbol{\xi}) \leq l_0$ implies $V_w \leq l_0$. Furthermore, according to *Lemma 1(iii)*, Ω is bounded. When $\|\boldsymbol{\xi}\| \rightarrow \infty$, then $V_w \rightarrow \infty$ according to *Lemma 1(ii)*, namely $V_1 \rightarrow \infty$.

- **Case 1: Obstacle is static.** (i) If $\mathbf{v}_o = \mathbf{0}$, then (34) becomes

$$\begin{aligned} \dot{V}_1 = & - \left(\text{sat} \left(k_1 \tilde{\boldsymbol{\xi}}_{wp}, v_m \right) - a_o \tilde{\boldsymbol{\xi}}_o \right)^T \\ & \cdot \text{sat} \left(\text{sat} \left(k_1 \tilde{\boldsymbol{\xi}}_{wp}, v_m \right) - a_o \tilde{\boldsymbol{\xi}}_o, v_m \right). \end{aligned} \quad (35)$$

In the following, we will show the convergence to the goal waypoint. The invariant set theorem is used to do the following analysis. Now, $\dot{V}_1 = 0$ if and only if

$$\text{sat} \left(k_1 \tilde{\boldsymbol{\xi}}_{wp}, v_m \right) - a_o \tilde{\boldsymbol{\xi}}_o = \mathbf{0} \quad (36)$$

according to (35). Then $\mathbf{v}_c = \mathbf{0}$ according to (28). Consequently, by (1), the system cannot get “stuck” at an equilibrium value except for $\mathbf{v} = \mathbf{0}$. The equation (36) can be further written as

$$k_1 \tilde{\mathbf{p}}_{wp} - a_o \tilde{\mathbf{p}}_o = \mathbf{0}. \quad (37)$$

According to equation (37), the equilibrium point \mathbf{p}^* obviously sits on the straight line through \mathbf{p}_{wp} and \mathbf{p}_o . As shown in Figure 6(a), the straight line is divided into: “A half-line”, “B segment” and “C half-line”. Obviously, the

equilibrium point \mathbf{p}^* cannot be on “A half-line” and “B segment” except for $\mathbf{p}^* = \mathbf{p}_{wp}$. Without loss of generality, it is assumed that the solution lying on “C half-line” is $\mathbf{p}^* = \bar{\mathbf{p}}$, as shown in Figure 6(b).

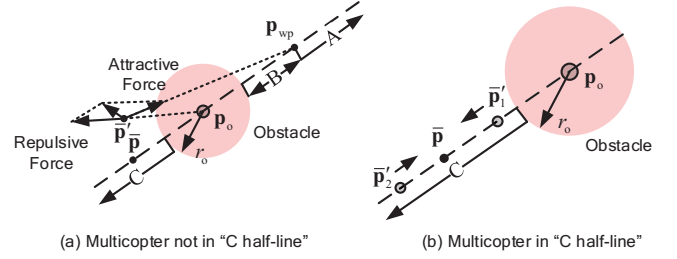


Fig. 6. Desired position generated for obstacle avoidance.

In the following, we will analyze the stability of $\bar{\mathbf{p}}$ on “C half-line”. By (37), we have

$$\frac{a_o}{k_1} = \frac{\|\tilde{\mathbf{p}}_{wp}\|}{\|\tilde{\mathbf{p}}_o\|} \quad (38)$$

at the equilibrium point $\mathbf{p} = \bar{\mathbf{p}}, \mathbf{v} = \mathbf{0}$. Since the solution lying on “C half-line”, $\|\tilde{\mathbf{p}}_{wp}\| = \|\tilde{\mathbf{p}}_o\| + \|\mathbf{p}_{wp} - \mathbf{p}_o\|$. Therefore, by (38), we have

$$a_o > k_1. \quad (39)$$

Let

$$\mathbf{f}(\boldsymbol{\xi}) = -k_1 \tilde{\boldsymbol{\xi}}_{wp} + a_o \tilde{\boldsymbol{\xi}}_o.$$

Then

$$\left. \frac{\partial \mathbf{f}(\boldsymbol{\xi})}{\partial \boldsymbol{\xi}} \right|_{\mathbf{p}=\bar{\mathbf{p}}, \mathbf{v}=\mathbf{0}} = (\Lambda + \mathbf{B})|_{\mathbf{p}=\bar{\mathbf{p}}, \mathbf{v}=\mathbf{0}}$$

where

$$\Lambda = (-k_1 + a_o) \mathbf{I}_2, \quad \mathbf{B} = \frac{\partial a_o}{\partial \|\tilde{\boldsymbol{\xi}}_o\|} \tilde{\boldsymbol{\xi}}_o \tilde{\boldsymbol{\xi}}_o^T \Big|_{\mathbf{p}=\bar{\mathbf{p}}, \mathbf{v}=\mathbf{0}}.$$

Since $\text{rank}(\mathbf{B}) = 1 < 2$ and $0 < \Lambda = \Lambda^T \in \mathbb{R}^{n \times n}$ is a symmetric positive-definite matrix by the fact (39), we have $\lambda_{\max} \left((\Lambda + \mathbf{B})|_{\mathbf{p}=\bar{\mathbf{p}}, \mathbf{v}=\mathbf{0}} \right) > 0$ according to *Lemma 4*. This implies, at the equilibrium point $\mathbf{p} = \bar{\mathbf{p}}, \mathbf{v} = \mathbf{0}$, the dynamics

$$\dot{\boldsymbol{\xi}} = \mathbf{f}(\boldsymbol{\xi})$$

is unstable because one of eigenvalues is positive. This does not imply the other eigenvalue is positive as well. If the other eigenvalue is negative, then the multicopter only can be stable in one dimensional space, which the measure is 0 on a 2D space. Therefore, we can conclude this proof when $\mathbf{v}_o = \mathbf{0}$.

- **Case 2: Obstacle is moving.** The proof is quite different from the proof above because, if $\mathbf{v}_o \neq \mathbf{0}$, the equilibrium point as well as its property are not easy to get from (34) directly. If $\mathbf{v}_o \neq \mathbf{0}$, then $\lim_{t \rightarrow \infty} \theta(t) = \pi$ for almost all $\tilde{\boldsymbol{\xi}}_o(0)$ by *Lemma 3*. This implies that there exists a time

²For all initial conditions $\tilde{\boldsymbol{\xi}}_{wp}(0)$, $\mathbf{p}_{wp,i}$ is a stable equilibrium with probability 1, and other equilibriums are unstable with probability 1.

$t_1 > 0$ such that $\|\mathbf{v}_o\| \|\tilde{\xi}_o\| \cos \theta = \tilde{\xi}_o^T(t) \mathbf{v}_o \leq 0$ for $t \geq t_1$. When $t_1 > 0$, (34) becomes

$$\begin{aligned} \dot{V}_1 \leq & - \left(\text{sat} \left(k_1 \tilde{\xi}_{wp}, v_m \right) - a_o \tilde{\xi}_o \right)^T \\ & \cdot \text{sat} \left(\text{sat} \left(k_1 \tilde{\xi}_{wp}, v_m \right) - a_o \tilde{\xi}_o, v_m \right) \end{aligned} \quad (40)$$

where the key step is to eliminate the term $a_o \tilde{\xi}_o^T \mathbf{v}_o$ of (34) by *Lemma 3*. The following proof is similar to that of *Case 1*. \square

Remark 5. We further explain why the multicopter cannot lie on “C half-line” intuitively. As shown in Figure 6(a), if the multicopter deviates from “C half-line”, for instance, it reaches $\mathbf{p}^* = \bar{\mathbf{p}}'$, then the sum of the attractive force and the repulsive force will make the multicopter further keep away from the “C half-line”. On the other hand, as shown in Figure 6(b), when the multicopter gets close to the obstacle along “C half-line”, for instance, it reaches $\mathbf{p}^* = \bar{\mathbf{p}}'_1$, the repulsive force will dominate because of the term $a_o \approx \frac{k_2}{\epsilon} \left\| \tilde{\xi}_o \right\|^3$ in the equation (28). As a result, a relatively large repulsive force will push it back to $\bar{\mathbf{p}}$. By contrary, if the multicopter reaches $\mathbf{p}^* = \bar{\mathbf{p}}'_2$, the attractive force will dominate. As a result, a relatively large attractive force will pull it back towards $\bar{\mathbf{p}}$. However, in practice, a multicopter will never strictly stay on “C half-line”, namely the measure of “C half-line” in 2D space equals 0 or the stability probability is 0. Therefore, any small deviation from the “C half-line” will drive the multicopter away from $\bar{\mathbf{p}}$. In conclusion, the solution $\mathbf{p}^* = \mathbf{p}_{wp}$ lying on “A half-line” is the only stable equilibrium point. It is also globally asymptotically stable with probability 1, namely $\lim_{t \rightarrow \infty} \|\tilde{\mathbf{p}}_{wp}(t)\| = 0$ for almost $\tilde{\mathbf{p}}_{wp}(0)$.

Remark 6. It is necessary to assume $v_m > v_o$. Otherwise, in the worst case, the collision cannot be avoided. For example, we can choose the obstacle dynamic as

$$\dot{\xi}_o = \dot{\xi} - \epsilon \frac{\xi_o - \xi}{\|\xi_o - \xi\|} \quad (41)$$

where $\|\dot{\xi}_o\| \leq \|\dot{\xi}\| + \epsilon_1 \leq v_m + \epsilon_1$ with $\epsilon_1 > 0$. From (41), it is easy to see $\|\xi_o(t) - \xi(t)\| < r_s + r_o$ within a finite time no matter how small ϵ_1 is. This implies that the obstacle is chasing after the multicopter and then hits it finally. It is worth pointing out the non-cooperate obstacle model considered in this paper has an unknown and unpredictable trajectory, but it has no intention of intercepting the multicopter (such as the obstacle always move to the line between the aircraft and the target point). The strategies of how to avoid such obstacles are further work. In theory, if the proposed obstacle model in this paper is used for analysis (with the exception of maximum speed, there are no more restrictions for them, such as the turning radius), it would be impossible to avoid these intercepted obstacles if the condition $v_m > v_o$ do not hold.

E. Result Extension to Multiple Moving Obstacles

The avoidance case with multiple non-cooperative moving obstacles is complex. Under some initial conditions, a multicopter cannot avoid collision with obstacles no matter what a controller uses, such as a case shown in Figure 7. However,

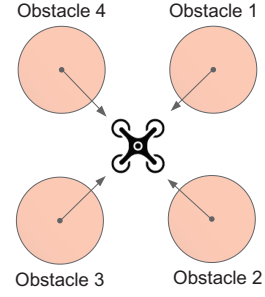


Fig. 7. A multicopter surrounded by four obstacles.

under some cases, the multiple moving obstacle avoidance control problem can be solved based on the results on the one moving obstacle avoidance control problem directly.

(1) Multiple Parallel Moving Obstacles with the Same Velocity

In practice, a multicopter will face a group of wild geese, which move with a constant velocity are parallel with each other. In order to adopt the proposed method, the clustered wild goose can be taken as one combined obstacle (as shown in Figure 8) with appropriate center position $\mathbf{p}_{o,c}$, velocity $\mathbf{v}_{o,c}$ and radius $r_{o,c}$. Define

$$\begin{aligned} \xi_{o,c} &= \mathbf{p}_{o,c} + \frac{1}{l} \mathbf{v}_{o,c} \\ \tilde{\xi}_{o,c} &= \xi - \xi_{o,c} \end{aligned}$$

The combined obstacle satisfies $\max \|\dot{\xi}_{o,c}\| \leq v_o$, $k = 1, \dots, N$. Similarly, we have *Assumption 2'* to replace with *Assumption 2* in the following.

Assumption 2'. The multicopter's initial filtered position $\tilde{\xi}_o(0) \in \mathbb{R}^2$ satisfies

$$\|\tilde{\xi}_{o,c}(0)\| > r_s + r_{o,c}$$

and $\|\mathbf{v}(0)\| \leq v_m$.

Based on *Assumptions 1, 2', 3*, the multiple moving obstacle problem can be degraded to the one moving obstacle avoidance control problem. As a result, the proposed method can still work.

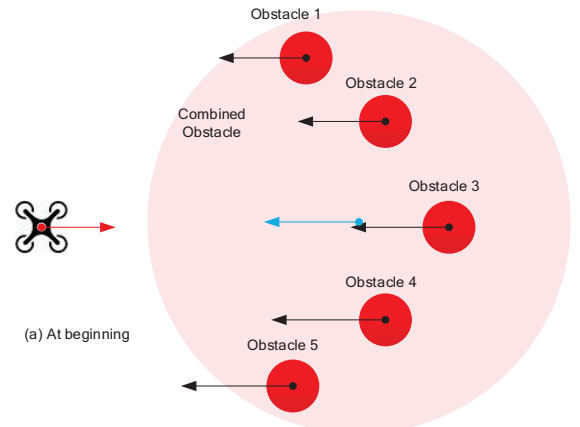


Fig. 8. Multiple clustered obstacles taken as a combined obstacle.

(2) Multiple Non-Parallel Moving Obstacles

At the same altitude, there are N moving obstacles

$$\mathcal{O}_{o,k} = \{\mathbf{x} \in \mathbb{R}^2 \mid \|\mathbf{x} - \mathbf{p}_{o,k}\| \leq r_{o,k}\}$$

where $\mathbf{p}_{o,k} \in \mathbb{R}^2$ is the center position of the k th obstacle, $\mathbf{v}_{o,k} = \dot{\mathbf{p}}_{o,k} \in \mathbb{R}^2$ is the velocity of the k th obstacle, $r_{o,k} > 0$ is the radius of the k th obstacle, $k = 1, \dots, N$. Define

$$\begin{aligned} \xi_{o,k} &= \mathbf{p}_{o,k} + \frac{1}{l} \mathbf{v}_{o,k} \\ \tilde{\xi}_{o,k} &= \xi_{o,k} - \xi_{o,k}. \end{aligned}$$

These obstacles satisfy $\max \|\dot{\xi}_{o,k}\| \leq v_o$, $k = 1, \dots, N$. To extend the conclusions to multiple moving obstacles, we have *Assumption 2''* to replace with *Assumption 2* in the following.

Assumption 2''. The multicopter's initial filtered position $\tilde{\xi}_o(0) \in \mathbb{R}^2$ satisfies

$$\|\tilde{\xi}_{o,k}(0)\| > r_s + r_{o,k}$$

and $\|\mathbf{v}(0)\| \leq v_m$, $k = 1, \dots, N$. The distances among obstacles satisfy

$$\|\mathbf{p}_{o,i}(t) - \mathbf{p}_{o,j}(t)\| \geq 2r_a + (r_{o,i} + r_{o,j}), i \neq j \quad (42)$$

then the multicopter cannot be close to two obstacles at the same time, namely

$$\mathcal{A} \cap \mathcal{O}_{o,i} \neq \emptyset, \mathcal{A} \cap \mathcal{O}_{o,j} \neq \emptyset$$

where $i \neq j$, $i, j = 1, \dots, N$.

Based on *Assumptions 1, 2'', 3*, the multicopter will encounter only one obstacle at any time so that the proposed method can still work. Here, each obstacle moves with a constant velocity, not paralleling with each other. After enough time, non-parallel obstacles must be separated far enough with each other. In this case, only one obstacle at most needs to be considered for the multicopter after enough time because the others are out of its avoidance area. The multiple moving obstacles problem can be degraded to the one moving obstacle avoidance control problem. As a result, the proposed method can still work. Let us discuss on the condition (42). If the condition (42) is not satisfied at some time, the multicopter is also safe if it is not at the place where two obstacles do not satisfy (42). Even if the multicopter will be the place, it can take these dangerous obstacles as one combined obstacle similar to the case of the multiple parallel moving obstacles. The strategies how to combine multiple obstacles are the further work.

Remark 7. If the multicopter and obstacles are *cooperative*, namely they make avoidance with each other, then multiple moving obstacles can keep away with each other and go to their waypoints finally. The dilemma shown in Figure 7 and the velocity constraint will not exist for the cooperative case. The formal proof is omitted here because of limited space. A simple explanation on the dilemma is that the other cooperative obstacles can keep away so that they satisfy *Assumption 2''*. On the other hand, the explanation on the velocity constraint is that the fast one is taken as the multicopter while the other taken as obstacles.

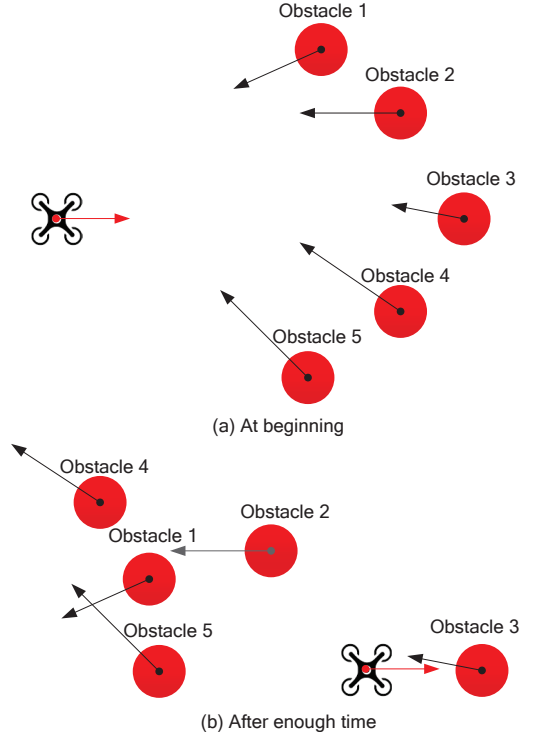


Fig. 9. Multiple non-parallel obstacles at the beginning and after enough time.

V. SIMULATION AND EXPERIMENT

Simulations and experiments are given in the following to show the effectiveness of the proposed method, where a video about simulations and experiments is available on <https://youtu.be/0kedvrRXUd8> or <https://suo.im/6wObz7>.

A. Simulation

We design three different scenarios to show the performance of the proposed controller. In the first scenario, the effectiveness of the proposed method to avoid one obstacle is shown. In the last two scenarios, the feasibility of the result extension to multiple obstacles is demonstrated.

(1) Simulation with One-on-One Non-Cooperative Obstacle

As shown in Figure 10 and Figure 11, two scenarios that one multicopter makes avoidance with one moving non-cooperative obstacle is considered. Because the condition $v_m > v_o$ holds, the taking over conflict can be ignored. We simulate the head on conflict and the converging conflict in two scenarios respectively. In the first designed scenario, as shown in Figure 10, the multicopter is facing a head on conflict, where the obstacle's velocity always points to the multicopter. The simulation parameters are set as follows. The multicopter with the safety radius $r_s = 5\text{m}$ and the avoidance radius $r_s = 7.5\text{m}$ is at $\mathbf{p}(0) = [0 \ 0]^T\text{m}$ initially. The waypoint $\mathbf{p}_{wp} = \mathbf{p}(0)$ is set to ensure that the multicopter is static initially. The multicopter has the maneuver constant $l = 5$, and the maximum speed $v_m = 6\text{m/s}$. The obstacle is at $\mathbf{p}_o(0) = [30 \ 0]^T\text{m}$ initially with radius $r_o = 10\text{m}$ and a constant velocity $\mathbf{v}_o = [-5 \ 0]^T\text{m/s}$. Under the initial conditions above and the proposed obstacle

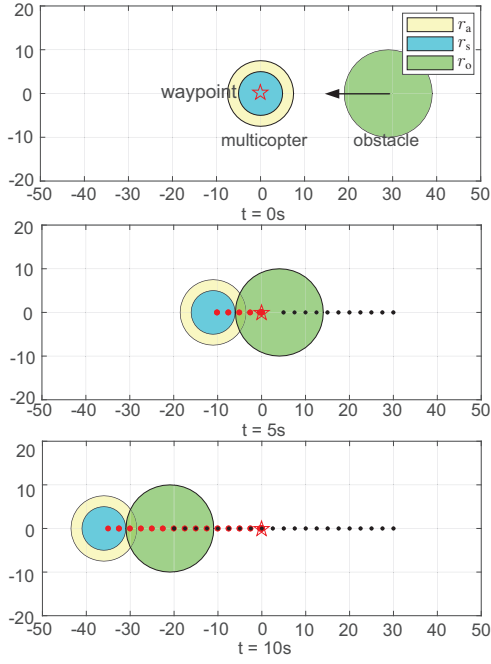


Fig. 10. Positions of UAV and obstacle at different times in head on conflict numerical simulation.

avoidance controller, the *filtered position distance* $\|\tilde{\xi}_{wp}(t)\|$ and $\|\tilde{\xi}_o(t)\|$ between the multicopter and the obstacle are shown in Figure 12. In this precisely constructed simulation scenario, the multicopter cannot arrive at the waypoint, which is with probability 0 in practice.

In the second designed scenario, as shown in Figure 11, the multicopter is facing a left converging conflict. We only change the initial positions and obstacle's constant velocity. The multicopter is at $\mathbf{p}(0) = [-30 \ 0]^T \text{m}$ initially and the waypoint $\mathbf{p}_{wp} = [30 \ 0]^T \text{m}$ is set, while the obstacle is at $\mathbf{p}_o(0) = [0 \ 30]^T \text{m}$ initially with a constant velocity $\mathbf{v}_o = [0 \ -5]^T \text{m/s}$. Under such conditions above and the proposed obstacle avoidance controller, the *filtered position distance* $\|\tilde{\xi}_{wp}(t)\|$ and $\|\tilde{\xi}_o(t)\|$ are shown in Figure 13. Therefore, the multicopter can avoid colliding the non-cooperative obstacle when facing different types of conflicts under the proposed controller.

(2) Simulation with Multiple Parallel Moving Obstacles with the Same Velocity

As shown in Figures 14-15, a scenario that one static multicopter makes avoidance with $N = 5$ parallel moving non-cooperative obstacles is considered. In this scenario, the obstacles are under homogeneous condition, similar to the horizon wall scenario proposed in [6]. The simulation parameters are set as follows. The multicopter with the safety radius $r_s = 5\text{m}$ and the avoidance radius $r_a = 7.5\text{m}$ is at $\mathbf{p}(0) = [20 \ -30]^T \text{m}$ initially. The multicopter has the maneuver constant $l = 5$, the maximum speed $v_m = 10\text{m/s}$ and the waypoint $\mathbf{p}_{wp} = [20 \ 30]^T \text{m}$. The obstacles are at $\mathbf{p}_{o,i}(0) = [15i - 45 \ 70 - 15|i - 3|]^T \text{m}$ initially with radius $r_{o,i} = 10 + 2i \text{m}$ and a constant velocity $\mathbf{v}_{o,i} = [0 \ -8]^T \text{m/s}$, $i = 1, \dots, N$. It is worth pointing out that these parallel

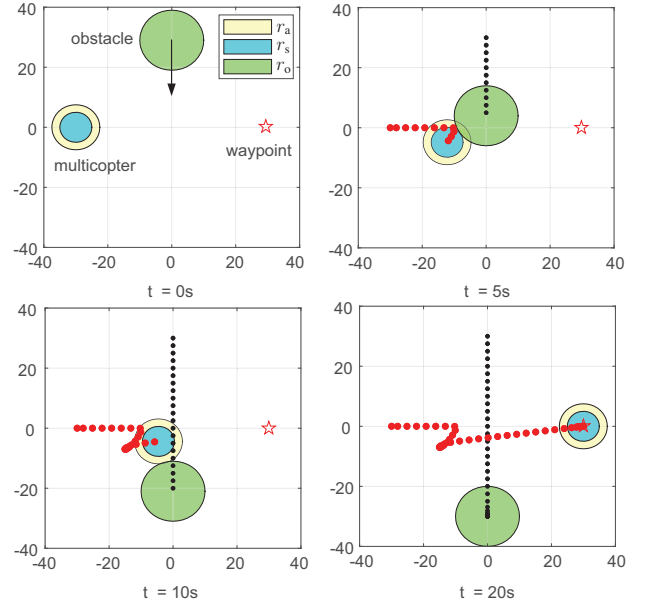


Fig. 11. Positions of UAV and obstacle at different times in left converge conflict numerical simulation.

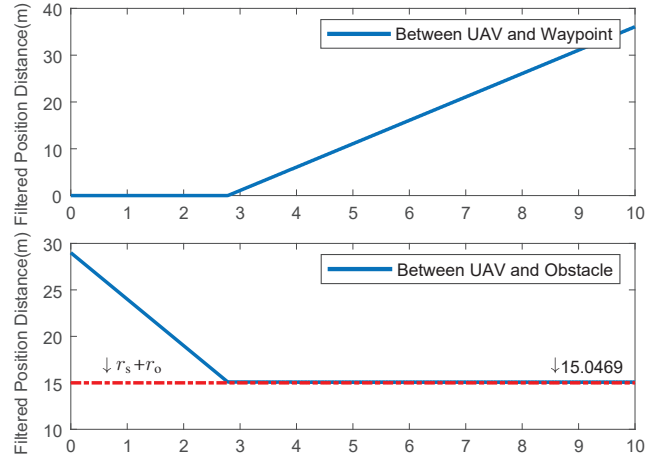


Fig. 12. The filtered position distance between UAV and waypoint, obstacle in head on conflict numerical simulation.

obstacles arrange in the “V” form with the same velocity. If we do not treat the parallel obstacles as a combined obstacle but use a traditional controller based on the artificial potential field method, as shown in Figure 14, the multicopter will be taken away by the moving obstacles, unable to arrive the goal waypoint. In this scenario, as shown in Figure 15, the obstacles can be taken as one combined obstacle with $r_{o,c} = 38.5\text{m}$, and *Assumption 2'* is satisfied. Under the initial conditions above and the proposed obstacle avoidance controller, the *filtered position distance* $\|\tilde{\xi}_{wp}(t)\|$, $\min_{i \in \{1, \dots, 5\}} \|\tilde{\xi}_{o,i}(t)\|$ and $\|\tilde{\xi}_{o,c}(t)\|$ are shown in Figure 16. Therefore, under the proposed controller, the multicopter can arrive at the goal waypoint while avoiding the parallel obstacles with the same velocity.

(3) Simulation with Multiple Non-Parallel Moving Obstacles

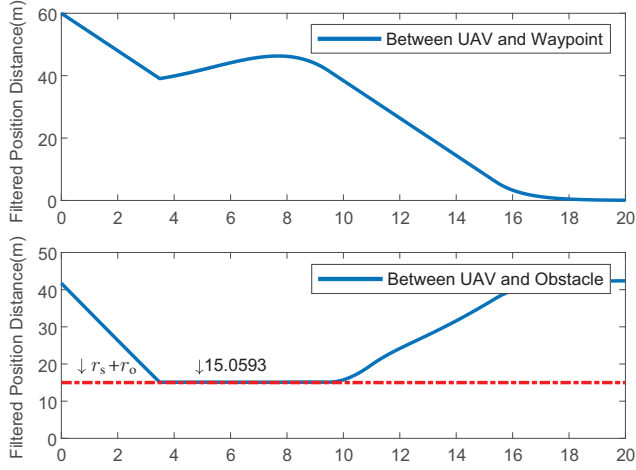


Fig. 13. The filtered position distance between UAV and waypoint, obstacle in left converge conflict numerical simulation.

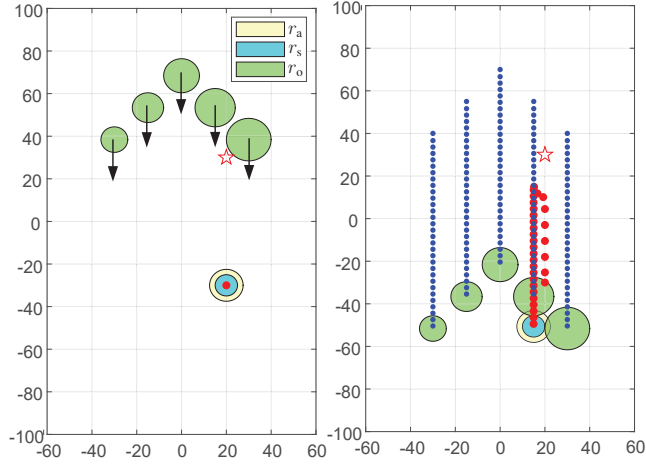


Fig. 14. Positions of UAV and obstacles at different times in numerical simulation.

As shown in Figure 17, a scenario that one static multicopter makes avoidance with $N = 4$ non-parallel moving non-cooperative obstacles is considered. In this scenario, the obstacles are under heterogeneous condition. The simulation parameters are set as follows. The multicopter with the safety radius $r_s = 5\text{m}$ and the avoidance radius $r_s = 7.5\text{m}$ is at $\mathbf{p}(0) = [50 \ -50]^T\text{m}$ initially. The multicopter has the maneuver constant $l = 5$, the maximum speed $v_m = 9\text{m/s}$ and the waypoint $\mathbf{p}_{wp} = [-50 \ 50]^T\text{m}$. The obstacles are with radius $r_{o,i} = 10 + 2i\text{m}$ and $v_o = 10\text{m/s}$, $i = 1, \dots, N$. These obstacles have unknown trajectories but satisfy *Assumption 2*". Under the initial conditions above and the proposed obstacle avoidance controller, the *filtered position distance* $\|\tilde{\xi}_{wp}(t)\|$, $\|\tilde{\xi}_{o,i}(t)\|$ and $\|\tilde{\xi}_{o,c}(0)\|$ are shown in Figure 18, $i = 1, \dots, N$. Therefore, under the proposed controller, the multicopter can arrive at the goal waypoint while avoiding the non-parallel obstacles.

(4) Simulation with Multiple Obstacles Using the Same Avoidance Controller

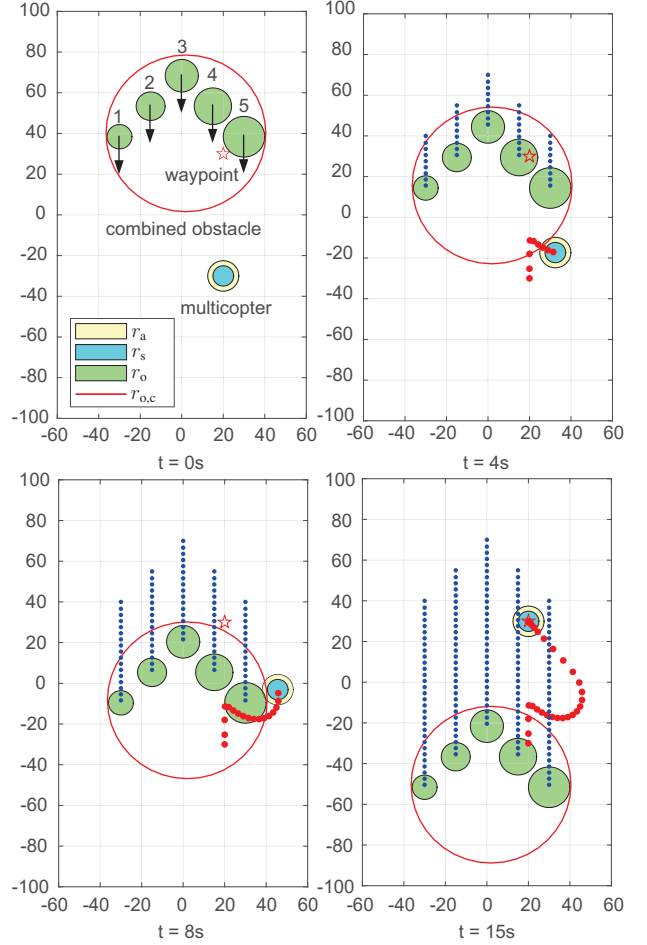


Fig. 15. Positions of UAV and combined obstacle at different times in numerical simulation.

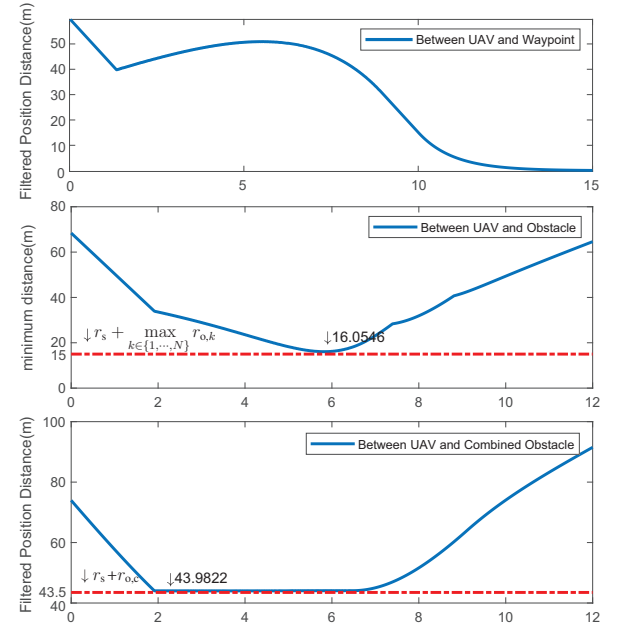


Fig. 16. The minimum filtered position distance between UAV and waypoint, obstacles in numerical simulation respectively.

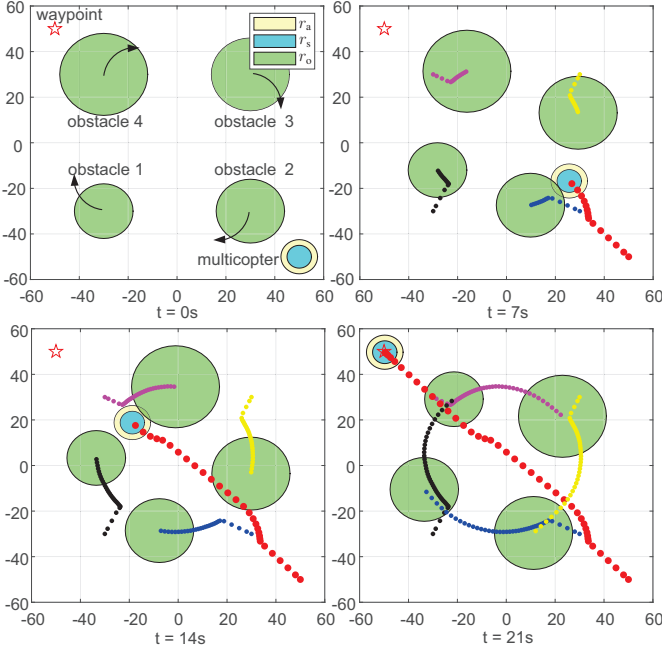


Fig. 17. Positions of UAV and obstacles at different times in numerical simulation.

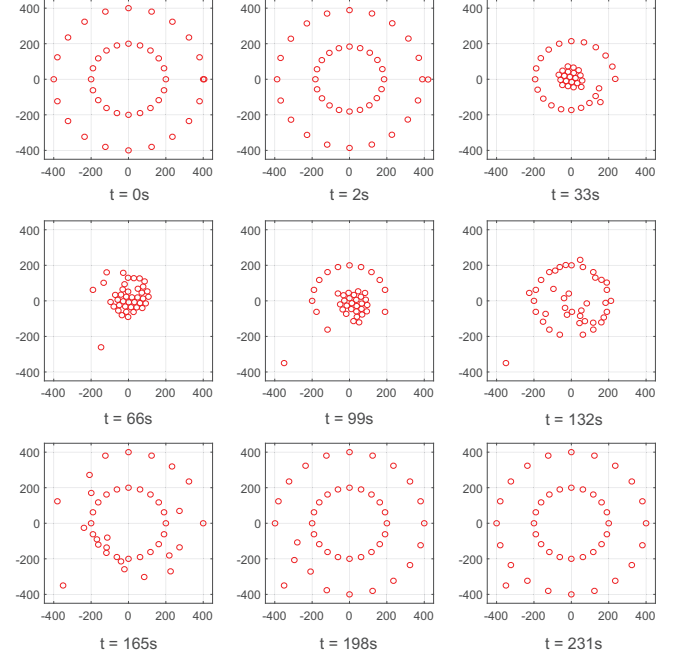


Fig. 19. Positions of 41 multicopters facing a super conflicts at different time

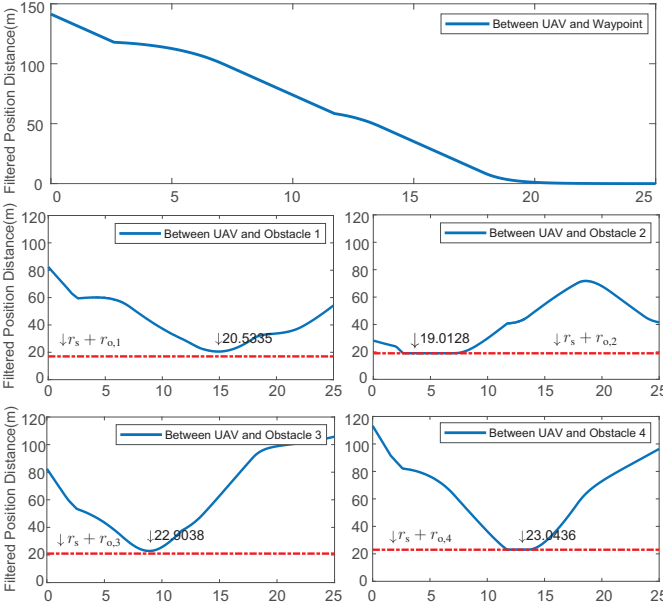


Fig. 18. The filtered position distance between UAV and waypoint, each obstacle in numerical simulation respectively.

A scenario of $M = 41$ multicopters with $r_s = 15\text{m}$, $r_a = 22.5\text{m}$ is considered, whose avoidance controllers are the same. The control gain $l_i = 5$ and the maximum speed of the i th multicopter $v_{m,i} = 5 + \frac{(i-1)}{8}\text{m/s}$, $i = 1, \dots, 41$. To simulate the super conflicts proposed in [6], for the i th multicopter, the

initial position and the waypoint are set as

$$\begin{cases} \mathbf{p}_i(0) = [400 \cos \frac{i-1}{10}\pi \ 400 \sin \frac{i-1}{10}\pi]^T \text{m}, i = 1, \dots, 20 \\ \mathbf{p}_{wp,i} = [400 \cos \frac{i+9}{10}\pi \ 400 \sin \frac{i+9}{10}\pi]^T \text{m} \\ \mathbf{p}_i(0) = [200 \cos \frac{i-1}{10}\pi \ 200 \sin \frac{i-1}{10}\pi]^T \text{m}, i = 21, \dots, 40. \\ \mathbf{p}_{wp,i} = [200 \cos \frac{i+9}{10}\pi \ 200 \sin \frac{i+9}{10}\pi]^T \text{m} \end{cases}$$

These positions are distributed on the circumference of two circles with center $\mathbf{o}_1 = \mathbf{o}_2 = [0 \ 0]^T$ and radius $r_1 = 400\text{m}$, $r_2 = 200\text{m}$, respectively. For the 41th multicopter, its initial position is set as $\mathbf{p}_{41}(0) = [405 \ 0]^T \text{m}$, which is closed to the 1st multicopter initially; the waypoint is $\mathbf{p}_{wp,41} = [-350 \ -350]^T \text{m}$. This is to simulate the situation a multicopter appears in another's safety area accidentally. As shown in Figures 19-20, each multicopter can fly to its waypoint without deadlock and conflict with other multicopters. The minimum distance among multicopters is shown in Figure 20. The minimum distance among multicopters is increased rapidly. At about $t = 2\text{s}$, the conflict between the 1st and the 41th multicopters has disappeared as soon as possible. From then on, no conflict happens again. The result shows that the multicopter can arrive at the goal waypoint while avoiding the obstacles under the proposed controller when the multicopter and the obstacles have the same avoidance controller.

B. Flight Experiment

A motion capture system called OptiTrack is installed, from which we can get the ground truth of the position, velocity and orientation of each multicopter. The laptop is connected to these multicopters and OptiTrack by a local network, providing the proposed controller and a real-time

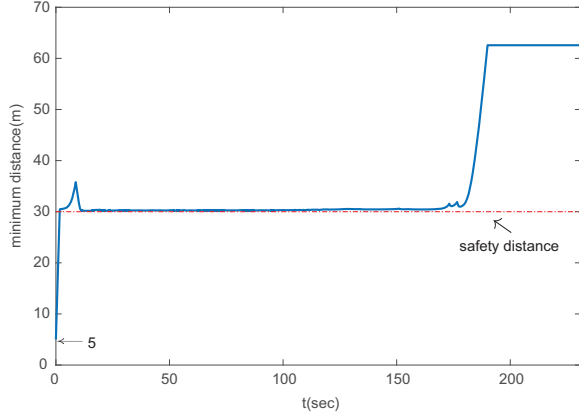


Fig. 20. Minimum distance among all multicopters facing a super conflicts

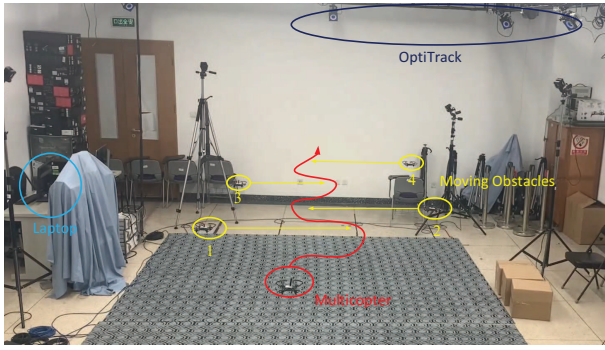


Fig. 21. Multiple moving obstacles with different directions.

position plotting module. In the two experiments, our design is similar to the last two simulation scenarios, assuming that $r_s = 0.2\text{m}$, $r_a = 0.25\text{m}$, $r_o = 0.2\text{m}$. The effectiveness of the proposed controller and the correctness of the result extension to multiple moving obstacles are further verified by the experiments.

(1) Multiple Parallel Moving Obstacles with Different Directions

As shown in Figure 21, the scenario contains one multicopter and $N = 4$ moving obstacles. The initial position and the waypoint of multicopter is set as $\mathbf{p}(0) = [0 \ -2.5]^T$ and $\mathbf{p}_{wp} = [0 \ 2.5]^T$ with $v_m = 0.12\text{m/s}$. The initial position of the i th obstacle $\mathbf{p}_{o,i}(0) = [(-1)^i \ i - 2]^T\text{m}$ and the velocity $\mathbf{v}_{o,i} = [0.1(-1)^{i+1} \ 0]^T\text{m/s}$ is set, $i = 1, \dots, N$. These obstacles satisfy *Assumptions 2'*. It is worth noting that the velocity direction for each obstacle is opposite to its neighboring obstacle. Therefore, similar to multiple non-parallel moving obstacles, the situation can be degraded to the one moving obstacle avoidance control problem. Finally, the multicopter can complete its route at 98s, keeping a safe distance from moving obstacles without conflict. The position of multicopter and obstacles during the whole flight experiment is shown in Figure 22.

(2) Multiple Parallel Moving Obstacles with the Same Velocity

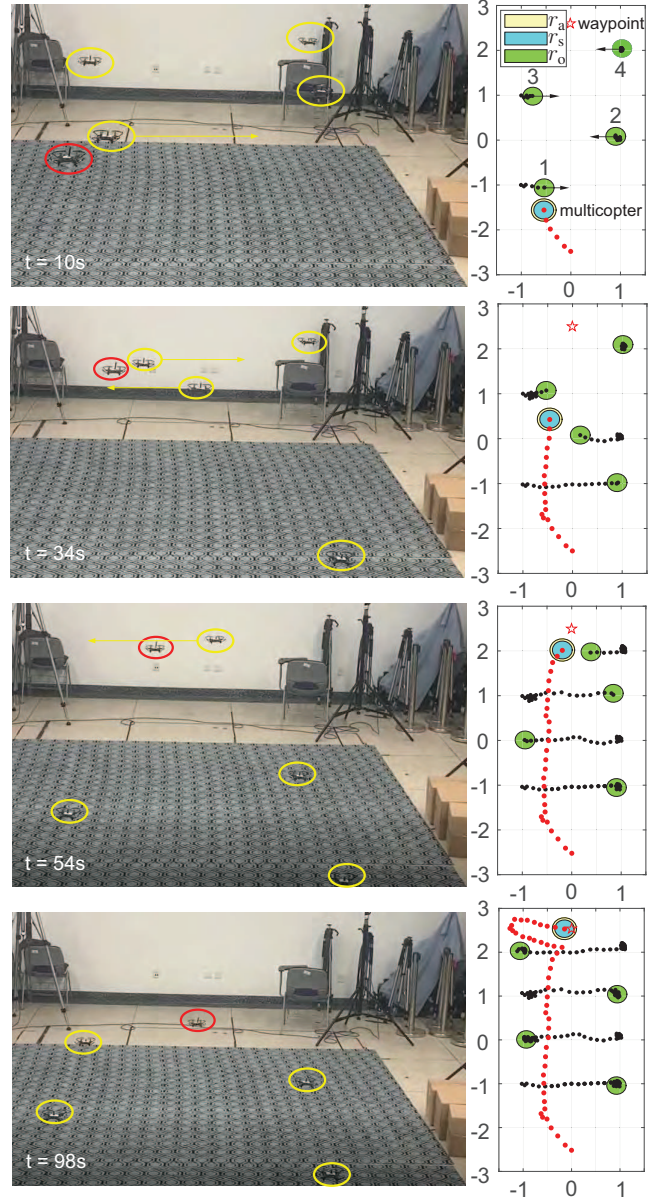


Fig. 22. Positions of UAV and obstacles in the case that multiple parallel moving obstacles with different directions.

As shown in Figure 23, the scenario contains one multicopter and $N = 3$ moving obstacles. The initial position and the waypoint of multicopter is set as $\mathbf{p}(0) = [0.3 \ -1]^T$ and $\mathbf{p}_{wp} = [0.3 \ 3]^T$ with $v_m = 0.12\text{m/s}$. The initial position and the velocity of the obstacle $\mathbf{p}_{o,i} = [2 - i \ 3 - 0.5|i - 2|]^T\text{m}$, $\mathbf{v}_{o,i} = [0 \ -0.1]^T\text{m/s}$ is set, $i = 1, \dots, N$. Similar to the simulation, these parallel obstacles arrange in a "V" shape. Under these conditions, these obstacles can be regarded as a combined obstacle while *Assumptions 2* is satisfied. Finally, the multicopter can complete its route at 34s, keeping a safe distance from these parallel moving obstacles without conflict. The position of multicopter and obstacles is shown in Figure 23.

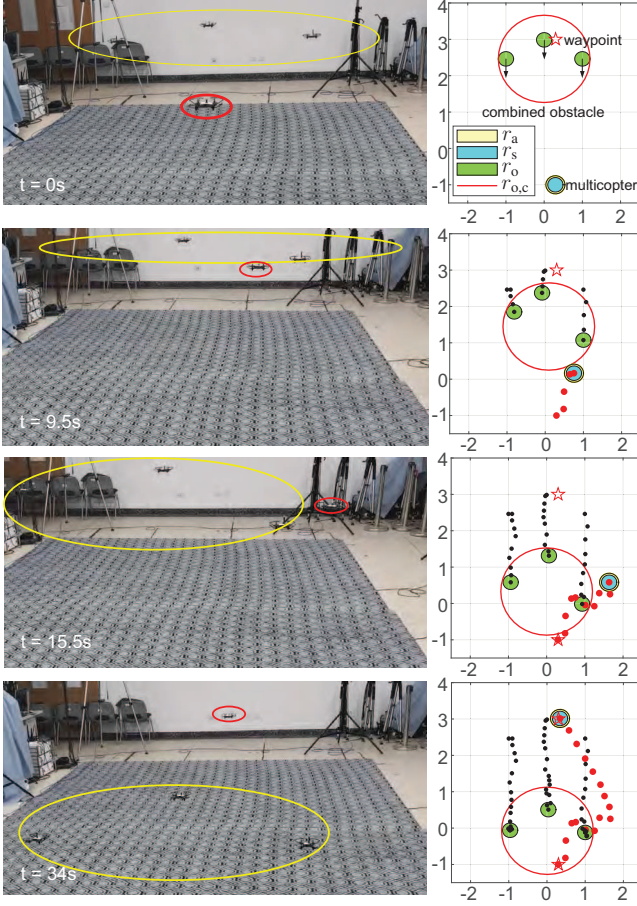


Fig. 23. Positions of UAV and obstacles in the case that multiple parallel moving obstacles with the same velocity.

VI. CONCLUSIONS

The moving non-cooperative obstacle avoidance problem is studied in this paper. First, a multicopter model and obstacle model are introduced. Since the multicopter's speed is confined, the necessary condition is to limit the velocity of non-cooperative moving obstacles. The force field method is used to solve the problem. During the controller design process, Lyapunov-like functions are designed with formal analysis and proofs, the instability about angle rather than position is proved for the case that the multicopter is in front of an obstacle moving direction, showing that one moving obstacle avoidance control problem can be solved. Furthermore, one moving obstacle avoidance control extends to two types of multiple moving obstacle avoidance control problems. Simulations and experiments are given to show the effectiveness of the proposed method from the functional requirement and the safety requirement. In the future, more studies are deserved to spend on developing strategies to deal with complex multiple moving obstacles.

VII. APPENDIX

A. Proof of Proposition 1

First, we have

$$\mathbf{v}^T \dot{\mathbf{v}} = -l \mathbf{v}^T \mathbf{v} + l \mathbf{v}^T \text{sat}(\mathbf{v}_c, v_m).$$

This implies

$$\frac{1}{2} \frac{d \|\mathbf{v}\|^2}{dt} = -l \|\mathbf{v}\|^2 + l \mathbf{v}^T \text{sat}(\mathbf{v}_c, v_m).$$

Consequently,

$$\frac{d \|\mathbf{v}\|}{dt} = -l \|\mathbf{v}\| + l \frac{1}{\|\mathbf{v}\|} \mathbf{v}^T \text{sat}(\mathbf{v}_c, v_m). \quad (43)$$

The solution to (43) is

$$\|\mathbf{v}(t)\| = e^{-lt} \|\mathbf{v}(0)\| + \int_0^t e^{-l(t-s)} \frac{l}{\|\mathbf{v}\|} \mathbf{v}^T \text{sat}(\mathbf{v}_c, v_m) ds.$$

Since $\|\text{sat}(\mathbf{v}_c, v_m)\| \leq v_m$, we have

$$\begin{aligned} \|\mathbf{v}(t)\| &\leq e^{-lt} \|\mathbf{v}(0)\| + \int_0^t e^{-l(t-s)} l v_m ds \\ &= e^{-lt} \|\mathbf{v}(0)\| + v_m (1 - e^{-lt}). \end{aligned}$$

With $\|\mathbf{v}(0)\| \leq v_m$, we have $\|\mathbf{v}(t)\| \leq v_m$, $t \geq 0$.

B. Proof of Proposition 2

(i) **Proof of sufficiency.** Let

$$\begin{aligned} p &= \tilde{\mathbf{p}}_o^T \tilde{\mathbf{p}}_o \\ \delta &= \tilde{\boldsymbol{\xi}}_o^T \tilde{\boldsymbol{\xi}}_o - \frac{1}{l^2} \tilde{\mathbf{v}}_o^T \tilde{\mathbf{v}}_o. \end{aligned}$$

According to (8), we have

$$\begin{aligned} \tilde{\boldsymbol{\xi}}_o^T \tilde{\boldsymbol{\xi}}_o &= \left(\tilde{\mathbf{p}}_o + \frac{1}{l} \tilde{\mathbf{v}}_o \right)^T \left(\tilde{\mathbf{p}}_o + \frac{1}{l} \tilde{\mathbf{v}}_o \right) \\ &= \tilde{\mathbf{p}}_o^T \tilde{\mathbf{p}}_o + \frac{1}{l^2} \tilde{\mathbf{v}}_o^T \tilde{\mathbf{v}}_o + \frac{2}{l} \tilde{\mathbf{v}}_o^T \tilde{\mathbf{p}}_o. \end{aligned} \quad (44)$$

Since

$$\frac{dp}{dt} = 2 \tilde{\mathbf{p}}_o^T \dot{\tilde{\mathbf{p}}}_o$$

using the equation (44), we further have

$$\frac{dp}{dt} = -lp + l\delta. \quad (45)$$

The solution $p(t)$ can be expressed as

$$p(t) = e^{-lt} p(0) + \int_0^t e^{-l(t-s)} l \delta(s) ds. \quad (46)$$

With (10) in hand, if condition (11) is satisfied, then

$$\delta(t) = \tilde{\boldsymbol{\xi}}_o^T \tilde{\boldsymbol{\xi}}_o - \frac{1}{l^2} \tilde{\mathbf{v}}_o^T \tilde{\mathbf{v}}_o \geq r^2.$$

Since $\|\tilde{\mathbf{p}}_o(0)\| > r$, we have $p(0) > r^2$. The solution in (46) satisfies

$$\begin{aligned} p(t) &\geq e^{-lt} r^2 + r^2 \int_0^t e^{-l(t-s)} l ds \\ &= r^2. \end{aligned}$$

Based on it, we have $\|\tilde{\mathbf{p}}_o(t)\| \geq r$, where $t \geq 0$. If $\frac{\mathbf{v}^T \mathbf{v}_o}{\|\mathbf{v}\| \|\mathbf{v}_o\|} = -1$, then the multicopter and the obstacle are in the case shown in Figure 1(b). Thus,

$$\frac{1}{l^2} \tilde{\mathbf{v}}_o^T \tilde{\mathbf{v}}_o = r_v.$$

Consequently, $\delta(t) = r^2$. Then, if $\|\tilde{\mathbf{p}}_o(0)\| = r$, then $\|\tilde{\mathbf{p}}_o(t)\| \equiv r$. Furthermore, if $\|\tilde{\xi}_o(t)\| > \sqrt{r^2 + r_v^2}$ and $\|\tilde{\mathbf{p}}_o(0)\| > r$, then $\|\tilde{\mathbf{p}}_o(t)\| > r$, where $t > 0$.

(ii) **Proof of necessity.** Given any $\epsilon_o > 0$, we will show if

$$\|\tilde{\xi}_o(t)\|^2 = r^2 + r_v^2 - \epsilon_o, \quad (47)$$

and $\|\tilde{\mathbf{p}}_o(0)\| = r$, then there exists a case that $\|\tilde{\mathbf{p}}_o(t)\| < r$, where $t \geq 0$. Consider a case $\frac{\mathbf{v}_o^T \mathbf{v}_o}{\|\mathbf{v}_o\| \|\mathbf{v}_o\|} = -1$. Then the multicopter and the obstacle are in the case shown in Figure 1(b). Thus,

$$\delta(t) = \tilde{\xi}_o^T \tilde{\xi}_o - \frac{1}{l^2} \tilde{\mathbf{v}}_o^T \tilde{\mathbf{v}}_o = r^2 - \epsilon_o.$$

According to (46), we have

$$p(t) = r^2 - \int_0^t e^{-l(t-s)} l \epsilon_o ds.$$

Therefore, $\|\tilde{\mathbf{p}}_o(t)\| < r$, where $t \geq 0$.

C. Proof of Lemma 2

First, we have

$$\dot{\tilde{\xi}}_o = -\text{sat}\left(\text{sat}\left(k_1 \tilde{\xi}_{wp}, v_m\right) - a_o \tilde{\xi}_o, v_m\right) - \mathbf{a}_o. \quad (48)$$

Since

$$\frac{d\tilde{\xi}_o^T \tilde{\xi}_o}{dt} = 2\tilde{\xi}_o^T \dot{\tilde{\xi}}_o$$

by using (48), we have

$$\frac{d\tilde{\xi}_o^T \tilde{\xi}_o}{dt} = -2\tilde{\xi}_o^T \text{sat}\left(\text{sat}\left(k_1 \tilde{\xi}_{wp}, v_m\right) - a_o \tilde{\xi}_o, v_m\right) - 2\tilde{\xi}_o^T \mathbf{a}_o. \quad (49)$$

We consider a case that, at time $t = t_1 > 0$, suppose

$$\|\tilde{\xi}_o(t_1)\| = (1 - \epsilon_\gamma) \gamma r_s + r_o \quad (50)$$

where $0 < \epsilon_\gamma < 1 - \frac{1}{\gamma}$ satisfies

$$1 < (1 - \epsilon_\gamma) \gamma < \gamma.$$

This implies no conflict at time t_1 . In this case, according to (27), we have

$$V_o(t_1) = \frac{k_2}{\epsilon \|\tilde{\xi}_o(t_1)\|^3} + g_1(\epsilon_s)$$

where $g_1(\epsilon_s)$ is a term related to $\epsilon_s > 0$ which satisfies $g_1(\epsilon_s) \rightarrow 0$ as $\epsilon_s \rightarrow 0$. As a result, according to definition of a_o ,

$$a_o \tilde{\xi}_o(t_1) = \left(\frac{k_2}{\epsilon \|\tilde{\xi}_o(t_1)\|^3} + g_2(\epsilon_s) \right) \tilde{\xi}_o(t_1)$$

where $g_2(\epsilon_s)$ is a term related to $\epsilon_s > 0$ satisfy $g_2(\epsilon_s) \rightarrow 0$ as $\epsilon_s \rightarrow 0$. Since ϵ is chosen very small, $a_o \tilde{\xi}_o$ dominates the

term $\text{sat}\left(k_1 \tilde{\xi}_{wp}, v_m\right) - a_o \tilde{\xi}_o$. Therefore, at time $t = t_1$, (49) becomes

$$\begin{aligned} \frac{d\tilde{\xi}_o^T \tilde{\xi}_o}{dt} &\geq 2\tilde{\xi}_o^T \text{sat}\left(\frac{k_2}{\epsilon \|\tilde{\xi}_o\|^3} \tilde{\xi}_o, v_m\right) - 2\tilde{\xi}_o^T \mathbf{a}_o \\ &\quad - |g_3(\epsilon_s)| - |g_4(\epsilon)| \\ &\geq 2\|\tilde{\xi}_o\| v_m - 2\|\tilde{\xi}_o\| \|\mathbf{a}_o\| - |g_3(\epsilon_s)| - |g_4(\epsilon)| \end{aligned} \quad (51)$$

where $g_3(\epsilon_s)$ is a term related to $\epsilon_s > 0$ which satisfies $g_3(\epsilon_s) \rightarrow 0$ as $\epsilon_s \rightarrow 0$, and $g_4(\epsilon)$ is a term related to $\epsilon > 0$ which satisfies $g_4(\epsilon) \rightarrow 0$ as $\epsilon \rightarrow 0$. Since

$$\frac{d\tilde{\xi}_o^T \tilde{\xi}_o}{dt} = \frac{d\|\tilde{\xi}_o\|^2}{dt} = 2\|\tilde{\xi}_o\| \frac{d\|\tilde{\xi}_o\|}{dt}$$

and $v_m > v_o$, by using (51), there exist sufficiently small $\epsilon_s, \epsilon > 0$ such that

$$\begin{aligned} \left. \frac{d\|\tilde{\xi}_o\|}{dt} \right|_{t=t_1} &\geq 2v_m - 2v_o - \frac{1}{(1 - \epsilon_\gamma) \gamma r_s + r_o} |g_3(\epsilon_s)| \\ &\quad - \frac{1}{(1 - \epsilon_\gamma) \gamma r_s + r_o} |g_4(\epsilon)|. \end{aligned}$$

There exist sufficiently small ϵ_s, ϵ such that

$$\begin{aligned} &2v_m - 2v_o - \frac{1}{(1 - \epsilon_\gamma) \gamma r_s + r_o} |g_3(\epsilon_s)| \\ &- \frac{1}{(1 - \epsilon_\gamma) \gamma r_s + r_o} |g_4(\epsilon)| > 0. \end{aligned}$$

This implies that if the filtered position error to the obstacle for the multicopter satisfies (50), the filtered position error will not be decreased any more. From the case, the filtered position error cannot be smaller than $(1 - \epsilon_\gamma) \gamma r_s + r_o$ anymore. Therefore, by using the fact $(1 - \epsilon_\gamma) \gamma r_s + r_o > r_s + r_o$, we can claim $\|\tilde{\xi}_o\| > r_s + r_o$.

D. Proof of Lemma 3

• **Step 1. A Lyapunov function defined.** Define

$$V_{1,1} = 1 + \frac{\tilde{\xi}_o^T \mathbf{v}_o}{\|\mathbf{v}_o\| \|\tilde{\xi}_o\|}.$$

According to (33), we have

$$\begin{aligned} V_{1,1} &= 1 + \cos \theta \\ &= 2 \cos^2 \frac{\theta}{2}. \end{aligned}$$

• **Step 2. Derivative of Lyapunov function.** The derivative of $V_{1,1}$ along the solution to (24) is

$$\begin{aligned} \dot{V}_{1,1} &= \frac{1}{\|\mathbf{v}_o\| \|\tilde{\xi}_o\|} \dot{\tilde{\xi}}_o^T \mathbf{P}_o \mathbf{v}_o \\ &= \frac{1}{\|\mathbf{v}_o\| \|\tilde{\xi}_o\|} \left(-\text{sat}\left(\text{sat}\left(k_1 \tilde{\xi}_{wp}, v_m\right) - a_o \tilde{\xi}_o, v_m\right) - \mathbf{v}_o \right)^T \mathbf{P}_o \mathbf{v}_o \end{aligned} \quad (52)$$

where

$$\mathbf{P}_o = \mathbf{I}_2 - \frac{\tilde{\xi}_o \tilde{\xi}_o^T}{\|\tilde{\xi}_o\|^2}.$$

By the definition of $\text{sat}(\cdot)$, we can rewrite the controller (28) as

$$\mathbf{v}_c = -\kappa_{v_{m,1}} \tilde{\xi}_{wp} + \kappa_{v_{m,2}} a_o \tilde{\xi}_o$$

where $\kappa_{v_{m,1}}, \kappa_{v_{m,2}} > 0$. Then $\dot{V}_{1,1}$ in (52) becomes

$$\begin{aligned} \dot{V}_{1,1} = & -\frac{1}{\|\mathbf{v}_o\| \|\tilde{\xi}_o\|} \mathbf{v}_o^T \mathbf{P}_o \mathbf{v}_o - \frac{\kappa_{v_{m,1}}}{\|\mathbf{v}_o\| \|\tilde{\xi}_o\|} \tilde{\xi}_{wp}^T \mathbf{P}_o \mathbf{v}_o \\ & + \frac{\kappa_{v_{m,2}} a_o}{\|\mathbf{v}_o\| \|\tilde{\xi}_o\|} \tilde{\xi}_o^T \mathbf{P}_o \mathbf{v}_o. \end{aligned}$$

Since $\tilde{\xi}_o^T \mathbf{P}_o \equiv 0$ according to the definition of \mathbf{P}_o , the derivative $\dot{V}_{1,1}$ further becomes

$$\dot{V}_{1,1} = -\frac{1}{\|\mathbf{v}_o\| \|\tilde{\xi}_o\|} \mathbf{v}_o^T \mathbf{P}_o \mathbf{v}_o - \frac{\kappa_{v_{m,1}}}{\|\mathbf{v}_o\| \|\tilde{\xi}_o\|} \tilde{\xi}_{wp}^T \mathbf{P}_o \mathbf{v}_o.$$

Since $\mathbf{v}_o \neq 0$ and the goal waypoint is static, then

$$\mathbf{p}_o - \mathbf{p}_{wp} = \mathbf{p}_o(0) + \mathbf{v}_o t - \mathbf{p}_{wp}.$$

Consequently,

$$\begin{aligned} \tilde{\xi}_{wp}^T \mathbf{P}_o \mathbf{v}_o &= \left(\tilde{\xi}_o + (\mathbf{p}_o - \mathbf{p}_{wp}) \right)^T \mathbf{P}_o \mathbf{v}_o \\ &= \tilde{\xi}_o^T \mathbf{P}_o \mathbf{v}_o + (\mathbf{p}_o - \mathbf{p}_{wp})^T \mathbf{P}_o \mathbf{v}_o \\ &= (\mathbf{p}_o - \mathbf{p}_{wp})^T \mathbf{P}_o \mathbf{v}_o \\ &= (\mathbf{p}_o(0) - \mathbf{p}_{wp})^T \mathbf{P}_o \mathbf{v}_o + t \mathbf{v}_o^T \mathbf{P}_o \mathbf{v}_o \end{aligned}$$

where $\tilde{\xi}_o^T \mathbf{P}_o \equiv 0$ is utilized. Therefore

$$\begin{aligned} \dot{V}_{1,1} = & -\frac{1}{\|\mathbf{v}_o\| \|\tilde{\xi}_o\|} \mathbf{v}_o^T \mathbf{P}_o \mathbf{v}_o \\ & - \frac{\kappa_{v_{m,1}} t}{\|\mathbf{v}_o\| \|\tilde{\xi}_o\|} \left(\frac{1}{t} (\mathbf{p}_o(0) - \mathbf{p}_{wp})^T \mathbf{P}_o \mathbf{v}_o \right. \\ & \left. + \mathbf{v}_o^T \mathbf{P}_o \mathbf{v}_o \right). \end{aligned} \quad (53)$$

Since

$$\dot{\tilde{\xi}}_o = -\text{sat} \left(\text{sat} \left(k_1 \tilde{\xi}_{wp}, v_m \right) - a_o \tilde{\xi}_o, v_m \right) - \mathbf{v}_o$$

we have

$$\|\dot{\tilde{\xi}}_o\| \leq v_m + \|\mathbf{v}_o\|.$$

Then

$$\begin{aligned} \|\tilde{\xi}_o\| &\leq \|\tilde{\xi}_o(0)\| + t(v_m + \|\mathbf{v}_o\|) \\ &\Rightarrow \\ 0 &< \frac{t}{\|\tilde{\xi}_o(0)\| + t(v_m + \|\mathbf{v}_o\|)} \leq \frac{t}{\|\tilde{\xi}_o\|}. \end{aligned}$$

Therefore, there exists a $t'_1 > 0$ such that

$$-\frac{t}{\|\tilde{\xi}_o\|} \leq -\frac{1}{2(v_m + \|\mathbf{v}_o\|)}, t \geq t'_1.$$

As a result, (53) becomes

$$\begin{aligned} \dot{V}_{1,1} &\leq -c_1 \mathbf{v}_o^T \mathbf{P}_o \mathbf{v}_o + \frac{1}{t} c_0 \|\mathbf{P}_o \mathbf{v}_o\| \\ &= -c_1 \|\mathbf{P}_o \mathbf{v}_o\|^2 + \frac{1}{t} c_0 \|\mathbf{P}_o \mathbf{v}_o\| \end{aligned} \quad (54)$$

where

$$\begin{aligned} c_0 &= \frac{\|\mathbf{p}_o(0) - \mathbf{p}_{wp}\|}{2 \|\mathbf{v}_o\| (v_m + \|\mathbf{v}_o\|)} \\ c_1 &= \frac{1}{\|\mathbf{v}_o\| \|\tilde{\xi}_o\|} + \frac{\kappa_{v_{m,1}}}{2 \|\mathbf{v}_o\| (v_m + \|\mathbf{v}_o\|)}. \end{aligned}$$

- **Step 3. Stability analysis.** The term $\mathbf{v}_o^T \mathbf{P}_o \mathbf{v}_o$ is rewritten as

$$\begin{aligned} \mathbf{v}_o^T \mathbf{P}_o \mathbf{v}_o &= \mathbf{v}_o^T \mathbf{v}_o - \frac{1}{\|\tilde{\xi}_o\|^2} \mathbf{v}_o^T \tilde{\xi}_o \tilde{\xi}_o^T \mathbf{v}_o \\ &= \mathbf{v}_o^T \mathbf{v}_o \sin^2 \theta \\ &= 4 \mathbf{v}_o^T \mathbf{v}_o \sin^2 \frac{\theta}{2} \cos^2 \frac{\theta}{2}. \end{aligned}$$

Since $\theta \in [0, \pi]$, $\sin \frac{\theta}{2} \cos \frac{\theta}{2} \geq 0$. Then

$$\begin{aligned} \|\mathbf{P}_o \mathbf{v}_o\| &= \sqrt{\mathbf{v}_o^T \mathbf{P}_o \mathbf{P}_o \mathbf{v}_o} = \sqrt{\mathbf{v}_o^T \mathbf{P}_o \mathbf{v}_o} \\ &= 2 \|\mathbf{v}_o\| \sin \frac{\theta}{2} \cos \frac{\theta}{2}. \end{aligned}$$

As a result, (54) becomes

$$\dot{V}_{1,1} \leq -W \left(\cos \frac{\theta}{2} \right).$$

where

$$\begin{aligned} W \left(\cos \frac{\theta}{2} \right) &= 4c_1 \|\mathbf{v}_o\|^2 \sin^2 \frac{\theta}{2} \cos^2 \frac{\theta}{2} \\ &\quad - \frac{2}{t} c_0 \|\mathbf{v}_o\| \sin \frac{\theta}{2} \cos \frac{\theta}{2}. \end{aligned}$$

There are only two solutions to make $W(\cos \frac{\theta}{2}) = 0$, namely $\theta = 0, \pi$. When $\theta = 0$, the Lyapunov function $V_{1,1}$ reaches its maximum, namely $V_{1,1} = 2$. When $\theta = \pi$, the Lyapunov function reach its minimum, namely $V_{1,1} = 0$. First, we will show that $\theta = 0$ is an unstable equilibrium. Given a perturbation $\Delta\theta > 0$ (it is noted that $\theta \in [0, \pi]$), there exists a sufficiently large $t_1 > 0$ such that

$$\sin \Delta\theta = 2 \sin \frac{\Delta\theta}{2} \cos \frac{\Delta\theta}{2} > \frac{c_0}{tc_1 \|\mathbf{v}_o\|}, t > t_1.$$

Then

$$W \left(\cos \frac{\Delta\theta}{2} \right) < 0.$$

This implies that $V_{1,1}$ will be decreased. Therefore, $\theta = 0$ is an unstable equilibrium. If

$$\sin \theta = 2 \sin \frac{\theta}{2} \cos \frac{\theta}{2} > \frac{c_0}{tc_1 \|\mathbf{v}_o\|}.$$

Then

$$W \left(\cos \frac{\theta}{2} \right) < 0.$$

It is noticed that $\frac{c_0}{t_{c1}\|\mathbf{v}_0\|} \rightarrow 0$ as $t \rightarrow \infty$. Similar to [34, Th 4.18], we can get $\sin \theta \rightarrow 0$ as $t \rightarrow \infty$. This implies $\lim_{t \rightarrow \infty} \theta(t) = \pi$. Only $\theta = \pi$ is a stable equilibrium. Even if the multicopter only can be stable in one dimensional space when $\theta = 0$, which the measure is 0 on a 2D space. Therefore, $\lim_{t \rightarrow \infty} \theta(t) = \pi$ for almost all $\tilde{\xi}_0(0)$.

E. Proof of Lemma 4

Proof. Since \mathbf{X} is a symmetric matrix with $\text{rank}(\mathbf{X}) \leq n-1$, the matrix \mathbf{X} can be written as

$$\mathbf{X} = \mathbf{V}^{-1} \text{diag} \begin{pmatrix} \lambda_1 & \cdots & \lambda_{n-1} & 0 \end{pmatrix} \mathbf{V}$$

where $\mathbf{V} \in \mathbb{R}^{n \times n}$ is the modal matrix, namely its columns are the eigenvectors of \mathbf{X} corresponding to eigenvalues $\lambda_1, \dots, \lambda_{n-1}, 0$. Then

$$\begin{aligned} \rho \mathbf{I}_n + \mathbf{X} &= \rho \mathbf{I}_n + \mathbf{V}^{-1} \text{diag} \begin{pmatrix} \lambda_1 & \cdots & \lambda_{n-1} & 0 \end{pmatrix} \mathbf{V} \\ &= \mathbf{V}^{-1} \text{diag} \begin{pmatrix} \rho + \lambda_1 & \cdots & \rho + \lambda_{n-1} & \rho \end{pmatrix} \mathbf{V}. \end{aligned}$$

Therefore, ρ is an eigenvalue of matrix $\rho \mathbf{I}_n + \mathbf{X}$. Consequently, $\lambda_{\max}(\rho \mathbf{I}_n + \mathbf{X}) \geq \rho > 0$. There exists a vector $\mathbf{x}_1 \in \mathbb{R}^n$ with $\|\mathbf{x}_1\| = 1$ such that [35, p. 176, Theorem (Rayleigh-Ritz)]

$$\begin{aligned} \lambda_{\max}(\rho \mathbf{I}_n + \mathbf{X}) &= \max_{\|\mathbf{x}\|=1} \mathbf{x}^T (\rho \mathbf{I}_n + \mathbf{X}) \mathbf{x} \\ &= \mathbf{x}_1^T (\rho \mathbf{I}_n + \mathbf{X}) \mathbf{x}_1 \geq \rho > 0. \end{aligned}$$

Then

$$\begin{aligned} \lambda_{\max}(\Lambda + \mathbf{X}) &= \max_{\|\mathbf{x}\|=1} \mathbf{x}^T (\Lambda + \mathbf{X}) \mathbf{x} \\ &\geq \mathbf{x}_1^T (\Lambda + \mathbf{X}) \mathbf{x}_1 \\ &= \mathbf{x}_1^T (\Lambda - \rho \mathbf{I}_n) \mathbf{x}_1 + \lambda_{\max}(\rho \mathbf{I}_n + \mathbf{X}). \end{aligned}$$

Since $\Lambda > \rho \mathbf{I}_n$, we have $\mathbf{x}_1^T (\Lambda - \rho \mathbf{I}_n) \mathbf{x}_1 > 0$. Consequently, $\lambda_{\max}(\Lambda + \mathbf{X}) > \rho > 0$.

REFERENCES

- [1] M. Gharibi, R. Boutaba, S.L. Waslander, "Internet of drones", *IEEE Access*, vol. 4, pp. 1148-1162, 2016.
- [2] S. Devasia and A. Lee, "Scalable low-cost unmanned-aerial-vehicle traffic network", *Journal of Air Transportation*, vol. 24, no. 3, pp. 74-83, 2016.
- [3] Y. I. Jenie, E. van Kampen, J. Ellerbroek, J. M. Hoekstra, "Taxonomy of Conflict Detection and Resolution Approaches for Unmanned Aerial Vehicle in an Integrated Airspace", *IEEE Transactions on Intelligent Transportation Systems*, vol. 18, no. 3, pp. 558-567, 2017.
- [4] M. Mitici, H. A. P. Blom, "Mathematical models for air traffic conflict and collision probability estimation", *IEEE Transactions on Intelligent Transportation Systems*, vol. 20, no. 3, pp. 1052-1068, 2019.
- [5] J. K. Kuchar and L. C. Yang, "A review of conflict detection and resolution modeling methods", *IEEE Transactions on Intelligent Transportation Systems*, vol. 1, no. 4, pp. 179-189, 2000.
- [6] J. M. Hoekstra and R. C. J. Ruigrok, R. N. H. W. Van Gent, "Free flight in a crowded airspace?", *Proceedings of the 3rd USA/Europe Air Traffic Management R&D Seminar*, 2001.
- [7] Y. Lin and S. Saripalli, "Sampling-based path planning for UAV collision avoidance", *IEEE Transactions on Intelligent Transportation Systems*, vol. 18, no. 11, pp. 3179-3192, 2017.
- [8] Y. I. Jenie, E. van Kampen, J. Ellerbroek, J. M. Hoekstra, "Safety Assessment of a UAV CD&R System in High Density Airspace Using Monte Carlo Simulations", *IEEE Transactions on Intelligent Transportation Systems*, vol. 19, no. 8, pp. 2686-2695, 2018.

- [9] S. Huang, R. S. H. Teo, K. K. Tan, "Collision avoidance of multi unmanned aerial vehicles: A review", *Annual Reviews in Control*, vol. 48, pp. 147-164, 2019.
- [10] A. Mcfadyen and L. Mejias, "A survey of autonomous vision-based see and avoid for unmanned aircraft systems", *Progress in Aerospace Sciences*, vol. 80, pp. 1-17, 2016.
- [11] E. R. Mueller and M. Kochenderfer, "Simulation comparison of collision avoidance algorithms for small multi-rotor aircraft", *AIAA Modeling and Simulation Technologies Conference*, pp. 3674, 2016.
- [12] P. Fiorini and Z. Shiller, "Motion planning in dynamic environments using velocity obstacles", *The International Journal of Robotics Research*, vol. 17, no. 7, pp. 760-772, 1998.
- [13] H. L. N. N. Thanh and S. K. Hong, "Completion of collision avoidance control algorithm for multicopters based on geometrical constraints", *IEEE Access*, vol. 6, pp. 27111-27126, 2018.
- [14] Y. I. Jenie, E.-J. van Kampen, C. C. de Visser, J. Ellerbroek, J. M. Hoekstra, "Selective velocity obstacle method for deconflicting maneuvers applied to unmanned aerial vehicles", *Journal of Guidance, Control, and Dynamics*, vol. 38, no. 6, pp. 1140-1146, 2015.
- [15] Y. I. Jenie, E.-J. van Kampen, C. C. de Visser, J. Ellerbroek, J. M. Hoekstra, "Three-dimensional velocity obstacle method for uncoordinated avoidance maneuvers of unmanned aerial vehicles", *Journal of Guidance, Control, and Dynamics*, vol. 39, no. 10, pp. 2312-2323, 2016.
- [16] H. Y. Ong and M. J. Kochenderfer, "Markov decision process-based distributed conflict resolution for drone air traffic management", *Journal of Guidance, Control, and Dynamics*, vol. 40, no. 1, pp. 69-80, Oct. 2016.
- [17] J. Saunders and B. Call, A. Curtis, R. Beard, T. McLain, "Static and dynamic obstacle avoidance in miniature air vehicles", *AIAA InfotechAerospace*, pp. 1-14, 2005.
- [18] S.M. LaValle and J.J. Kuffner, "Randomized kinodynamic planning", *International Journal of Robotics Research*, vol. 20, no. 5, pp. 378-400, 2001.
- [19] B. Balázs and G. Vásárhelyi, "Coordinated dense aerial traffic with self-driving drones", *2018 IEEE International Conference on Robotics and Automation (ICRA)*, pp. 6365-6372, 2018.
- [20] C. Virágh, M. Nagy, C. Gershenson, G. Vásárhelyi, "Self-organized UAV traffic in realistic environments", *2016 IEEE/RSJ International Conference on Intelligent Robots and Systems (IROS)*, pp. 1645-1652, 2016.
- [21] E. G. Hernandez-Martinez and E. Aranda-Bricaire, "Convergence and collision avoidance in formation control: A survey of the artificial potential functions approach", *Multi-Agent Systems—Modeling Control Programming Simulations and Applications*, pp. 103-126, 2011.
- [22] E. Boivin, A. Desbiens and E. Gagnon, "UAV collision avoidance using cooperative predictive control", *2008 16th Mediterranean Conference on Control and Automation*, pp. 682-688, 2008.
- [23] X. Yang and P. Wei, "Autonomous on-demand free flight operations in urban air mobility using Monte Carlo tree search", *2018 8th International Conference for Research in Air Transportation*, 2018.
- [24] A. Richards and J. P. How, "Aircraft trajectory planning with collision avoidance using mixed integer linear programming", *2002 American Control Conference (IEEE Cat. No. CH37301)*, vol. 3, pp. 1936-1941, 2002.
- [25] A. Alonso-Ayuso, L. F. Escudero, F. J. Martín-Campo, "Collision avoidance in air traffic management: A mixed-integer linear optimization approach", *IEEE Transactions on Intelligent Transportation Systems*, vol. 12, no. 1, pp. 47-57, 2011.
- [26] Y. Lin and S. Saripalli, "Collision avoidance for UAVs using reachable sets", *2015 International Conference on Unmanned Aircraft Systems (ICUAS)*, pp. 226-235, 2015.
- [27] Y. Rasekhipour, A. Khajepour, S. Chen, B. Litkouhi, "A potential field-based model predictive path-planning controller for autonomous road vehicles", *IEEE Transactions on Intelligent Transportation Systems*, vol. 18, no. 5, pp. 1255-1267, 2017.
- [28] Q. Quan, *Introduction to Multicopter Design and Control*, Singapore:Springer, 2017.
- [29] D. Panagou, D. M. Stipanović, P. G. Voulgaris, "Distributed coordination control for multi-robot networks using Lyapunov-like barrier functions", *IEEE Transactions on Automatic Control*, vol. 61, no. 3, pp. 617-632, 2016.
- [30] D. Šišlák, P. Volf, M. Pěchouček, "Agent-based cooperative decentralized airplane-collision avoidance", *IEEE Transactions on Intelligent Transportation Systems*, vol. 12, no. 1, pp. 36-46, 2011.
- [31] DJI, "Hardware Introduction"[Online], Available:<https://developer.dji.com/onboard-sdk/documentation/introduction/osdk-hardware>

- [32] J.-J. E. Slotine and W. Li, *Applied Nonlinear Control*, Englewood Cliffs, NJ:Prentice Hall, 1991.
- [33] G. B. Thomas, M. D. Weir, J. Hass, C. Heil, *Thomas' Calculus*, Boston, MA, USA:Pearson, 2014.
- [34] H. K. Khalil, *Nonlinear Systems*, New Jersey, NJ, USA:Prentice-Hall, vol. 3, 1996.
- [35] R. A. Horn and C. R. Johnson, *Matrix Analysis*, Cambridge, U.K.:Cambridge University Press, 2012.



Quan Quan received the B.S. and Ph.D. degrees in control science and engineering from Beihang University, Beijing, China, in 2004 and 2010, respectively. He has been an Associate Professor with Beihang University since 2013, where he is currently with the School of Automation Science and Electrical Engineering. His research interests include reliable flight control, vision-based navigation, repetitive learning control, and timedelay systems.



Rao Fu received the B.S. degree in control science and engineering from Beihang University, Beijing, China, in 2017. He is working toward to the Ph.D. degree at the School of Automation Science and Electrical Engineering, Beihang University (formerly Beijing University of Aeronautics and Astronautics), Beijing, China. His main research interests include UAV traffic control and swarm.



Kai-Yuan Cai Kai-Yuan Cai received the B.S., M.S., and Ph.D. degrees in control science and engineering from Beihang University (Beijing University of Aeronautics and Astronautics), Beijing, China, in 1984, 1987, and 1991, respectively. He has been a Full Professor with Beihang University since 1995. He is a Cheung Kong Scholar (Chair Professor), appointed by the Ministry of Education of China in 1999. His main research interests include software testing, software reliability, reliable flight control, and software cybernetics.